TRIPOLI-5 /MENDEL coupling and application to a Nuclear Thermal Propulsion reactor assembly

In collaboration with

Master's Degree in Energy and Nuclear Engineering

Candidate

Thomas BORSELLO

Supervisors

Thibault MOULIGNIER

Dr. Roland LENAIN

Prof. Sandra DULLA

ACADEMIC YEAR 2025/2026

Abstract

This work was carried out as part of a research internship at the French Alternative Energies and Atomic Energy Commission (CEA) in the SERMA/LPEC department. The thesis focuses on Nuclear Thermal Propulsion (NTP) and investigates the SNRE (Small Nuclear Reactor Engine) concept derived from the NERVA program.

Nuclear Thermal Propulsion (NTP) systems are incredibly interesting for future space explorations, such as crew-operated Mars missions. Compared to conventional chemical propulsion systems, NTP offers several key advantages such as a higher specific impulse, which results in greater efficiency, thrust and shorter travel times for the same distance. The reactor investigated in this thesis is the NERVA reactor SNRE, that is able to bring together the best characteristics of previous NTP reactor concepts, enhancing overall performance and mission suitability. It uses a lightweight propellant, hydrogen, which can be heated directly by a high-temperature fission reaction to generate thrust. The main aspect studied is how the fuel composition changes in time by coupling the CEA Monte Carlo transport code TRIPOLI-5 with the CEA depletion code MENDEL.

This coupling aims to enable detailed transient fuel depletion analysis within the SNRE engine, investigating on the reactor's criticality and the project feasibility. The integration of the two codes is carried out exploting the the ICoCo interface and the C3PO library, developed at CEA, which coordinates data exchange and controls the overall flow. Thanks to the modular structure and simplicity of the implementation, the coupling framework remains both user-friendly and adaptable, making it easier to apply to other reactor concepts or extend with additional physical models.

Acknowledgements

This internship represents the final step of my long university journey and the beginning of my professional career. I would like to take this opportunity to express my sincere gratitude to those who supported and guided me along the way.

I would like to sincerely thank my tutor, Thibault, who made the start of the internship much easier by accepting both my gaps and strengths with patience and support, and by supporting me throughout the entire experience.

Many thanks also to Roland, whose outstanding coding skills helped me during the most challenging phases of the internship.

I am also grateful to Professor Sandra Dulla, who provided me with a solid background in nuclear physics and related subjects, and who was the one to first propose this internship opportunity to me.

6 months away from home and loved ones are not easy and have not been easy, but I have to thank my colleagues at CEA that decreased the stress by creating a heartwarming place where working became more joyful.

A heartfelt thank you goes to my family, my girlfriend, and my friends. Your constant, genuine, and unconditional support has meant the world to me. Despite the distance, you never made me feel truly far, and for that, I will always be grateful.

Table of Contents

List of Tables

List of Figures

1 | Introduction

1.1 Background and context

In recent decades Nuclear Thermal Propulsion (NTP) systems have regained significant attention for future space exploration, particularly for crew-operated Mars missions. Compared to conventional chemical propulsion systems, NTP can offer a higher specific impulse and consequently a higher propulsion efficiency and a lower travel time for the same distance and propellant mass. In a NTP engine the propellant, typically hydrogen, is directly heated by the energy released by the fission reaction and successively expanded through a nozzle to create thrust. In this context, neutronics analysis and the fuel evolution play a central role, since the system performance and operability depend on the reactor criticality and on the core behaviour.

During the 1960s, the development of Nuclear Thermal Propulsion systems was the focus of extensive research in the United States [1], mainly in the Rover and NERVA programs. The objective of these programs was the demonstration of the technical feasibility of rocket engines powered by nuclear reactors, able to heat hydrogen at very high temperatures and to obtain better performances compared to conventional chemical propulsion systems. Multiple reactor prototypes were developed and experimentally tested, showing that nuclear reactors could operate under conditions compatible with space propulsion applications.

Despite the termination of the NERVA program in the early 1970s, mainly due to political, safety and strategic reasons, the concept of NTP has continued to attract interest in the scientific community. In recent years, the interest has grown again due to possible human missions to Mars, for which reducing travel time, by improving propulsion efficiency, is a crucial factor. In this context, the study of neutron behaviour inside the reactor and of the isotopic evolution over time becomes particularly important. Indeed, during reactor operation, the isotopic composition of the fuel changes due to fission, neutron capture and decay mechanisms. This evolution directly affects the reactor reactivity, the generation of fission products

and, therefore, the efficiency of the propulsion system. To correctly describe these phenomena, it is necessary to combine a neutron transport code with a depletion code. The integration of these simulation tools represents the key element to correctly study and assess the NTP performance and feasibility.
This thesis was developed during a curricular internship at CEA (Commissariat à l'énergie atomique et aux énergies alternatives), in the SERMA/LPEC department, which focuses on nuclear science and technology. The case study investigated is the NERVA reactor SNRE (Small Nuclear Reactor Engine) [1], selected for its characteristics and historical and technical interest related to NTP systems. The main focus of the work is on the temporal variation of the fuel composition and on the consequences related to it on reactivity k_{eff}, neutron production, fission product generation and residual power after shutdown.

1.2 Aim of the thesis

The general aim of the thesis is the development, implementation and verification of the coupling between a neutron transport Monte Carlo code (TRIPOLI-5) and a depletion code (MENDEL) to study the transient behaviour and evolution of the fuel in an NTP reactor concept of the SNRE type.
More specifically, the goals are:

1. **Define** and **develop** a **coupling** workflow based on **ICoCo and C3PO**, able to manage and coordinate the execution of the codes and the exchanged data in a standardized manner.

2. **Exchange** the **required quantities** between the two codes, transferring the properly processed **flux spectrum** from TRIPOLI-5 to MENDEL and returning to TRIPOLI-5 the newly evaluated **isotopic concentrations** at each time step.

3. **Maintain a modular and reusable implementation**, extendable to other reactor concepts or additional physics through dedicated driver, exchanger and coupler components.

4. **Apply the coupling to the SNRE case study**, evaluating k_{eff}, neutron production and isotopic composition, assessing the impact of the coupled approach with respect to the uncoupled one.

5. Perform a **verification of the coupling** on a simplified benchmark problem with the comparison against a TRIPOLI-4-based reference solution.

1.2.1 Thesis outline

To guide the reader, the thesis is organized as follows:

- **Chapter 1 – Introduction:** background, context and aim of the thesis
- **Chapter 2 – Propulsion system and NERVA projects:** background on propulsion systems and an overview of NTP and NERVA concepts.
- **Chapter 3 – Neutronics and the TRIPOLI-5 Code:** overview of neutronics, description of the Monte Carlo method and of the SNRE geometrical model with stand-alone results.
- **Chapter 4 – MENDEL depletion code:** overview of depletion, stand-alone results, and examples of computed quantities, including decay heat considerations.
- **Chapter 5 – Coupling structure:** ICoCo/C3PO architecture and implementation of the data-exchange and time-marching workflow.
- **Chapter 6 – Results:** application to SNRE with discussion of k_{eff}, isotopic inventories, decay heat, and modelling assumptions.
- **Chapter 7 – Verification:** comparison against the TRIPOLI-4 reference and assessment of steady-state and depletion consistency.
- **Chapter 8 – Conclusions and perspectives:** summary of the work and possible future developments.

2 | Propulsion system and NERVA projects

In this chapter, the fundamentals of Nuclear Thermal Propulsion (NTP) are introduced, together with an overview of the NERVA program and related reactor concepts. The SNRE (Small Nuclear Reactor Engine) case study considered in this thesis is then presented, with emphasis on its main design features relevant to the analyses performed in the following chapters.

2.1 Propulsion system overview

Propulsion systems A propulsion system is a mechanism designed to move an object generating thrust through the conversion of thermal energy into kinetic energy [2]. Energy is produced from the combustion reaction of chemical propellants (usually fuel and oxidizer) into a combustion chamber, creating gases at high temperatures that are successively expanded in a supersonic nozzle. The components of a space propulsion system can be summarized as follows:

- **Storage system**, stores the fuel and the oxidizers at low temperature to prevent their boil-off
- **Propellant feed system**, which takes the propellant from the storage system, providing it to the heating system at sufficient pressure. It is usually composed by a compressor, a turbine, some valves and the combustion chamber
- **Heating system**, whose job is the warming up of the propellant
- **Expanding nozzle**, which expands and accelerates the heated gas generating thrust

Thrust production Thrust is produced when the hot gases are expanded and accelerated in the nozzle, exploiting the Third Newton law.

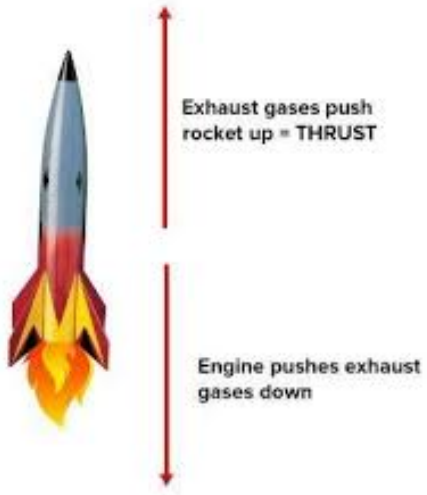

Figure 2.1: Third Newton Law on a space rocket [3]

As Figure 2.1 shows, by expelling gas backwards at high speed, the vehicle is pushed forward with an equal and opposite force:

$$F = \dot{m} v_e \tag{2.1}$$

$\dot{m}$ is the mass flow rate and v_e the exhaust speed which can be evaluated, assuming an ideal gas, in the case of a convergent-divergent De Laval nozzle with:

$$v_e = \sqrt{\frac{2\gamma}{\gamma - 1} \frac{R \cdot T}{M} \left[1 - \left(\frac{p_e}{p} \right)^{\frac{\gamma - 1}{\gamma}} \right]} \tag{2.2}$$

In Equation 2.1 the parameters are:

- v_e: exhaust velocity
- R: universal gas law constant
- M: gas molar mass
- T: combustion chamber temperature
- γ: ratio of specific heats c_p/c_v
- p: absolute pressure of inlet gas
- p_e: absolute pressure of the gas at nozzle exit

2.2 NTP systems

Nuclear Thermal Propulsion (NTP) systems are propulsion systems that unlike the conventional chemical ones, use a small nuclear reactor as kernel of the engine. The reason why the interest was so high was due to its high specific impulse that is about twice that the chemical, making the space trips faster and further with the same amount of propellant.

$$I_{sp} = \frac{v_e}{g_0} = \frac{1}{g_0} \cdot \sqrt{\frac{2\gamma}{\gamma - 1} \cdot \frac{RT}{M}} \tag{2.3}$$

The formula of the specific impulse 2.3 depends on:

- γ: isotropic expansion factor
- R: universal gas law constant
- T: gas temperature
- M: gas molar mass
- v_e: Exhaust gas velocity
- g_0: standard gravity

and highlights the reason behind the high specific impulse observed in NTP systems. Compared to other propulsion systems, the temperature of the propellant is low, but the gas molar mass is much smaller due to the fact that only LH2 is used, that has $M = 2$.

System	**Gas**	**Molar Mass M (g/mol)**	**Temperature T (K)**	**Specific Impulse I_{sp} (s)**
RS-25	LH_2 / LOx	15	3300	452
Raptor	LOx / kerosene	23.3	3500*	350
NERVA	LH_2	2	2700	900

Table 2.1: Comparison of Propulsion Systems [4], [5]

The chamber temperature of the Raptor engine was nowhere to be found in technical official reports.

The core historically uses a UZrC-C graphite composite and uses liquid hydrogen (LH_2) both as coolant and as propellant. The propellant cycle can be summarized as follows.
LH2 is first pumped from the storage tank by a turbo-pump. The flow is then divided into two streams:

1. **Cooling and turbopump drive loop**
    - LH_2 cools the nozzle, increasing its temperature and becoming a super-critical gas
    - The cold H_2 gas, cools down the reflector and the moderator
    - The heated H_2 gas, at a temperature of a few hundred kelvin, is then used to drive the turbopump
2. **Main flow**
    - This flow will mix with the heated H_2 before entering the reactor core

The combined flow then passes through the core, removing heat. The H_2, hotter than 2400 K, extends through the nozzle producing thrust.

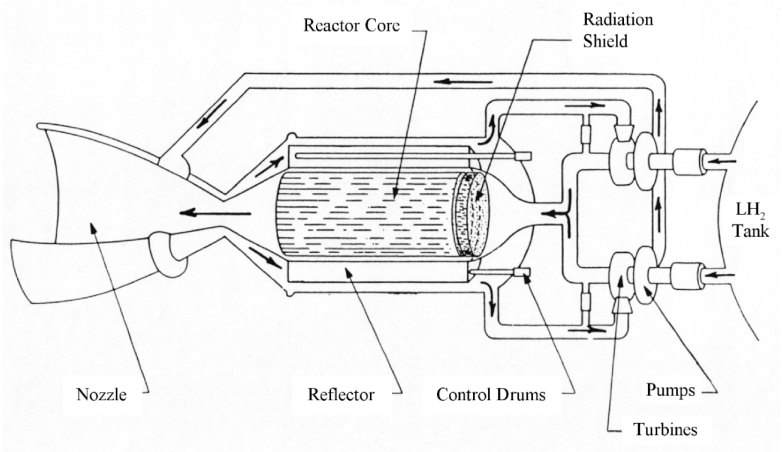

Figure 2.2: NTP general layout [6]

A general schematic layout of a NTP system is shown in Figure 2.2. Its main components can be summarized as follows [7]:

- **Hydrogen propellant tanks**, where cryogenic temperature liquid hydrogen is stored
- **Propellant delivery feed system**, which comprehends all the devices needed to ensure the right flow of the propellant through the reactor

- **Fuel assembly**, which contains the fissile material and the fuel cladding
- **Tie tube assembly**, which serve both as moderator by slowing down the prompt neutrons and as a structural component, preventing the breaking apart or ejection of the fuel elements
- **Control plates**, made either by B_4C or BCu, able to control the reaction, keep the criticality and sustain the chain process. They can be tilted to increase the reactivity inserted.
- **Reflector**, needed to decrease the leakage probability
- **Nozzle**, where the propellant is expelled
- **Internal and external shield**, needed to reduce the gamma and neutron flux levels in engine components located ahead of the reactor

As shown in the LH_2 cycle, several components, including the moderator, reflector, and nozzle, also contribute to preheating the coolant before it enters the turbine.

2.3 NERVA program

The most significant effort to study and develop an NTP system was the NERVA program. The Nuclear Engine for Rocket Vehicle Application (NERVA) was started in 1955 by NASA/Los Alamos when the Atomic Energy Commission (AEC) assigned Lawrence Livermore labs Project Pluto (code name Tory) for nuclear ramjets and Los Alamos Project Rover for nuclear rockets.

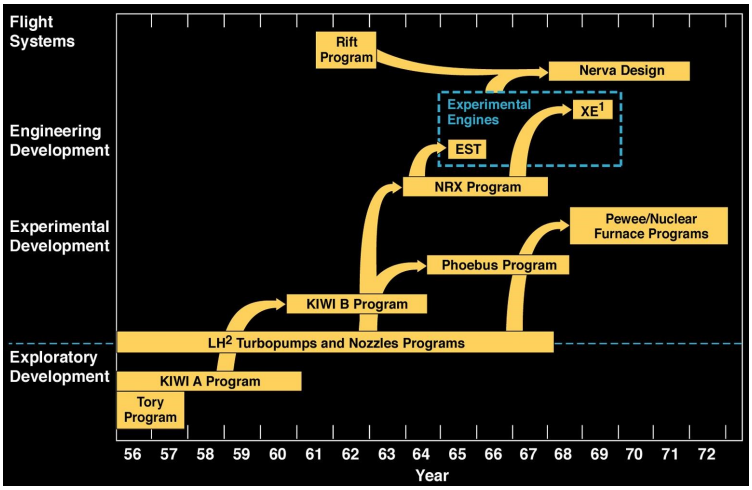

Figure 2.3: NERVA program history [1]

The projects was divided in the research program and the actual reactor and engines tests, as can be appreciated in Figures 2.3 and 2.4. The research program can be summarized as it follows:

- **KIWI Program**, developed to test NTP principles. There were multiple KIWI reactor design: KIWI-A whose focus was on the core integrity and neutronics, KIWI-B that introduces the hydrogen propellant flow and the KIWI-TNT that tested reactor containment failure modes
- **PHOEBUS Program**, devised to push the power limit of the NTP systems, achieving a thermal power of 5 GWth
- **PEWEE Program**, needed to study more compact engine and to increase their operational time
- **Nuclear Furnace 1**, to test ceramic fuel at operational conditions

In the meantime, full scale reactor demonstrations have been carried out, notably:

- **NRX tests**, spread on 6 different reactor configuration. These tests progressively incorporated advancements and feedback from the research and development programs
- **XE-Prime reactor**, that showed a good reliability, controllability (being able to be restarted multiple times) and promising thrust and specific impulse

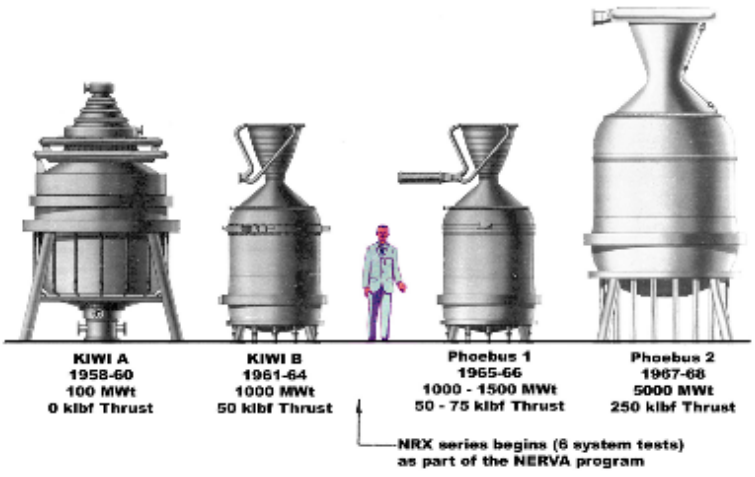

Figure 2.4: NERVA Test Program [1]

In 1972 funding was cut off, leading to the end of the program and to the stopping of all further testing.

2.4 Small Nuclear Reactor Engine

The most promising design, which would likely have been selected if the program had continued is based on the Pewee test and Nuclear Furnace experiments. The Pewee test was characterized by the most compact engine while achieving the highest power density, whereas the Nuclear Furnace tested the first composite fuel elements. The SNRE design, which combines these two developments, is used as the case study in this report. Its fuel elements and tie tubes have a hexagonal cross-section, resulting in a core arranged in a hexagonal lattice, as can be seen in Figure 2.5.

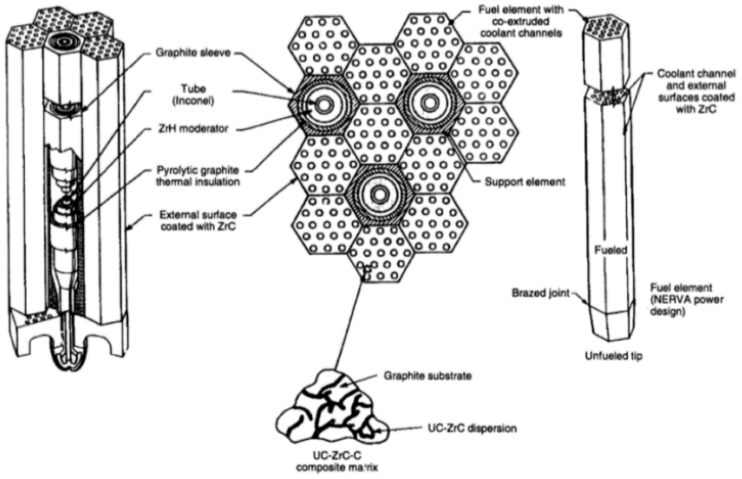

Figure 2.5: Hexagonal element disposition [8]

All the informations related to the material data and compositions are provided in Annex and Chapter 3 along with an in depth study of the neutrons behaviour.

These are the characteristics of the reactor:

Fuel element

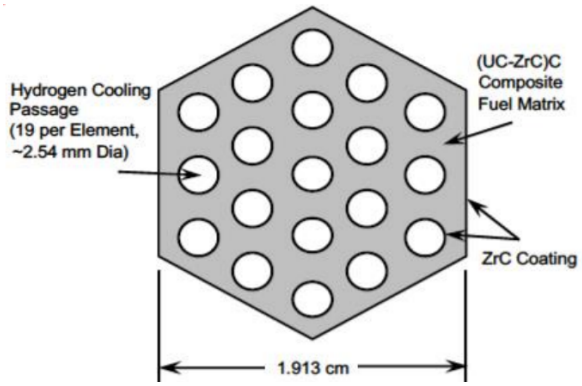

Figure 2.6: Fuel element [8]

Table 2.2: Fuel element data [8]

Element	Size (cm)
Pitch	1.913
H_2 radius	0.127
Coat width	0.01
Height	88.9

Tie tube element

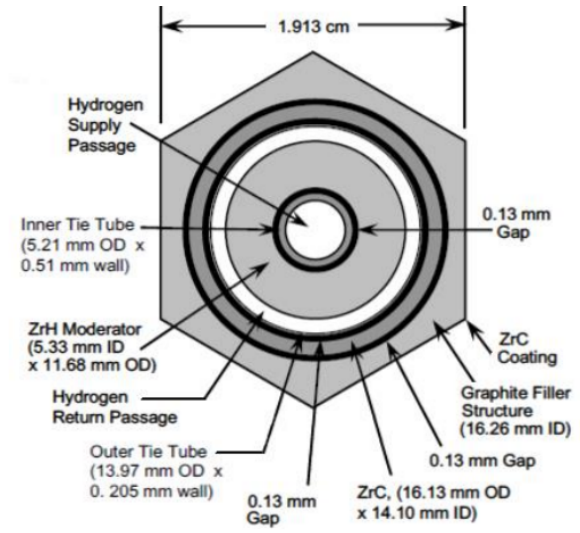

Figure 2.7: Tie tube element [8]

Table 2.3: Tie tube element data [8]

Element	Size (cm)
Pitch	1.913
H_2 supply radius	0.2095
Inner tie tube radius	0.2605
Gap_1 radius	0.2665
$ZrH_{1.89}$	0.584
H_2 return radius	0.678
Outer tie tube radius	0.6985
Coat radius	0.8065
Gap_2	0.8195
Height	88.9

The core is composed of 564 fuel elements and 241 tie tubes, that when summed up lead to 805 elements in the reactor. Each tie tube is surrounded by fuel elements, to improve as much as possible their moderating and cooling capabilities, Figure 2.8.

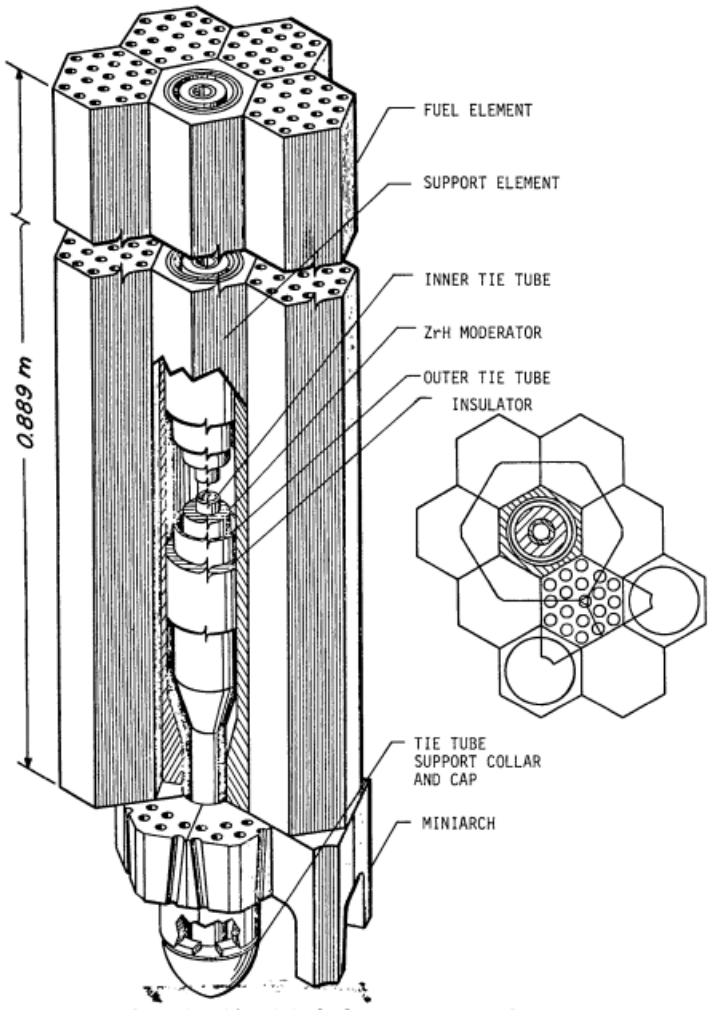

Figure 2.8: Tie surrounding [9]

Reflector

The primary purpose of the reflector is to minimize neutron leakage from the core. It is composed of several components, but for simplicity, this study focuses only on the sector assemblies, control drum assemblies, and the beryllium barrel.

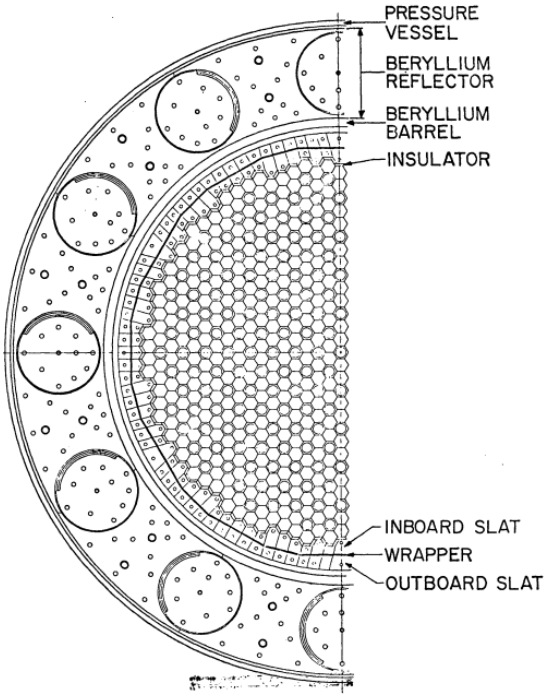

Figure 2.9: Transverse section of the reflector assembly [9]

Table 2.4: Reflector assembly data [9]

Element	Size (cm)
Reflector inner radius	33.65
Barrel thickness	1
Reflector thickness	14.7
Vessel thickness	0.559
Drum radius	5.461

Control Plates Figure 2.9 also shows the control plate system, which consists of 12 absorbent plates, arranged around the core periphery in the reflector assembly, each covering about 120° of arc. They are used to regulate the fission chain reaction by absorbing neutrons:

Element	Size (cm)
Control plate thickness	0.961136
Control plate arc	120°

Table 2.5: Control plates data [9]

In summary, this chapter covered the propulsion system basics, an overview of Nuclear Thermal Propulsion systems, especially the NERVA program and the Small Nuclear Reactor Engine. These topics are an essential background for the following analysis. The following chapter presents the neutronics basic, the stochastic Monte Carlo method and its implementation in the TRIPOLI-5 code, which is applied to the reactor model examined in this study.

3 | Neutronics and the TRIPOLI-5 Code

In this chapter the basics of neutronics and of the Monte Carlo method will be explained, along with the TRIPOLI-5 representation of all the elements in the reactor. Finally, the standalone result of TRIPOLI-5 will be provided and commented.

3.1 Neutronics theory

3.1.1 General overview

In the context of nuclear reactors, neutronics refers to the study of the behaviour of neutrons in matter, focusing on their production, movement and interaction inside a reactor core. A key part of this branch of science is analyzing the various kind of reaction that can take place when a neutron interact with a nucleus.

Reactions This paragraph discusses the reactions that can take place when a neutron interact with a nucleus.

Atoms consist of a nucleus made of protons and neutrons, called nucleons, surrounded by electrons. Neutrons are neutral subatomic particles that can be emitted by several nuclear reactions, and can interact with other atoms. Due to their small size, the interaction between them and other subatomic particles is not taken into account.
Different reactions can take place when a neutron hits a nucleus, and they can be summarized as follows:

- **Fission reaction:** the nucleus splits into two smaller nuclei (sometimes three), releasing energy and more neutrons

- **Capture reaction:** the nucleus absorbs the neutron, becoming a heavier isotope without splitting

- **Scattering reaction:** the neutron collides with the nucleus and bounces off, possibly transferring energy but not being absorbed

Cross section Each reaction is characterized by a probability per unit path length of taking place, known as the macroscopic cross section, denoted by Σ $[cm^{-1}]$. There is a cross section per possible reaction, which can be summed in three categories, scattering Σ_s, fission Σ_f and capture Σ_c. The fission and capture cross sections together make up the absorption cross section:

$$\Sigma_\mathrm{a} = \Sigma_\mathrm{c} + \Sigma_\mathrm{f} \tag{3.1}$$

since both processes involve the absorption of a neutron by the nucleus.
The macroscopic cross section is related to the microscopic cross section σ [cm^2] or *barn* [b] ($1\,\mathrm{b} = 10^{-24}\,\mathrm{cm}^2$) and the number of target nuclei per unit volume N, that has the dimension of nuclei/cm^3. To find this nuclei density, knowing the mass of the nuclide A and its density ρ:

$$N = \frac{N_\mathrm{A} \cdot \rho}{A} \tag{3.2}$$

where N_A is Avogadro's number. [10]

Scattering Nuclear scattering can be divided into two main categories:

- **Elastic scattering**, where the incident particle and the target nucleus remain in their original states. There is no transformation or destruction of either particle, and the total kinetic energy of the system is conserved.

$$\mathrm{n} + {}^{238}\mathrm{U} \rightarrow \mathrm{n} + {}^{238}\mathrm{U}$$

- **Inelastic scattering**, where part of the kinetic energy is converted into excitation energy of the nucleus, with consequent release of a gamma photon.

$$\mathrm{n} + {}^{56}\mathrm{Fe} \rightarrow \mathrm{n} + {}^{56}\mathrm{Fe}^* \rightarrow \mathrm{n} + {}^{56}\mathrm{Fe} + \gamma$$

The scattering process plays a key role in most nuclear reactors, since it is able to slow down neutrons leading to a higher probability for U-235 to undergo fission, as we will see later. Materials that perform this function are called **moderators**,

as they reduce the velocity, and therefore the energy, of the incident particle. In elastic scattering some of the neutron's energy is transferred to the nucleus, leading to a slowing down of the neutron. This transfer is higher when the atomic mass is similar to that of the incident particle, so the ideal target nucleus, as well as the most used, are Hydrogen and Carbon. This fast energy reduction is crucial since we would like the slowdown to be as fast as possible to avoid capture by other nuclei, such as Uranium-238.

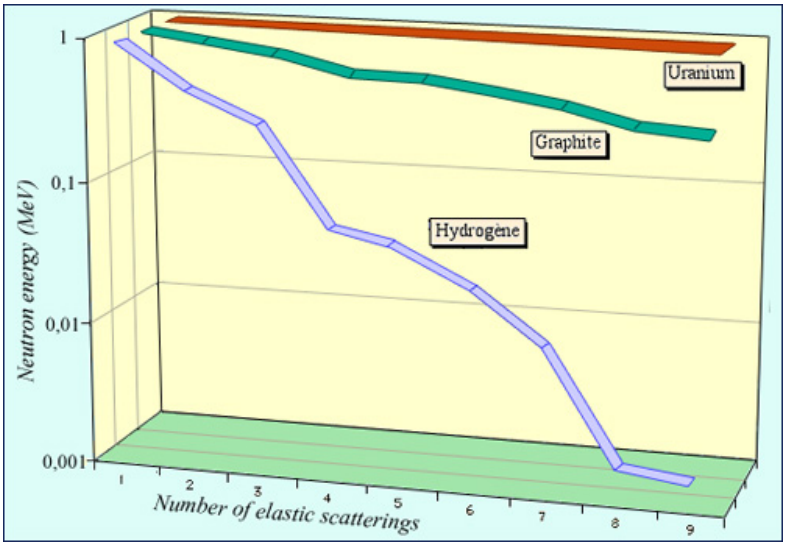

Figure 3.1: Moderator capabilities [11]

As can be seen in Figure 3.1, Hydrogen is able, in less than 10 elastic scatterings, to slow down the neutron by a factor of 1000. On average, it takes about 26 collisions to thermalize a 2 MeV neutron in a hydrogenated environment, 31 in deuterium, 120 in carbon, and 2202 in uranium [11].

Capture Capture is the reaction in which a neutron is absorbed by a nucleus. This will make an heavier isotope, that eventually can become unstable and split. The most common and important types are:

- **Radiative neutron capture** (n, γ), where the neutron is absorbed by the nucleus, forming an excited compound nucleus that subsequently emits a gamma photon.

$$\mathrm{n} + {}^{59}\mathrm{Co} \rightarrow {}^{60}\mathrm{Co} + \gamma$$

- **(n, 2n) reaction**, in which an incoming neutron induces the emission of two neutrons from the target nucleus.

$$n + {}^{27}Al \rightarrow 2\,n + {}^{26}Al$$

- **Neutron-induced charged particle emission**, less common, in which the capture of a neutron causes the emission of a charged particle such as a proton or an alpha particle.

$$n + {}^{14}N \rightarrow {}^{14}C + p$$
$$n + {}^{10}B \rightarrow {}^{7}Li + \alpha$$

Neutron capture in nuclear reactors plays a significant role in two key aspects: it directly affects reactivity and the evolution of fuel composition over time. Reactivity control in a nuclear reactor is mandatory to be able to keep the fission reaction chain under control. Neutron absorbers are the components able to perform this job. The most used and studied neutron absorber materials are:

- **Boron (B):** primarily boron-10, used both in control rods and soluble boron in PWRs' coolant [12]
- **Gadolinium (Gd):** Gd-155 and Gd-157 have incredibly high neutron absorption cross-section. They are mainly used as burnable absorbers during the start-up of the reactor or as emergency shutdown [12]
- **Cadmium (Cd):** used in control rods [12]

In this kind of absorber, the lower the energy of the incident neutron, the higher their capture cross section, as can be seen in the figure below:

The evolution of the fuel during reactor operation is a significant process that must be carefully considered. Neutron capture can transform fissionable material into fissile material. Fissionable material refers to any nucleus that can undergo fission if struck by a particle with a sufficiently high energy, such as a fast neutron, to overcome the nuclear binding energy barrier. In contrast, a fissile material is any nuclide that can undergo fission with thermal neutrons and therefore can sustain a chain reaction. The most common reaction is the one of Uranium-238:

$$n + {}^{238}U \rightarrow {}^{239}U \rightarrow {}^{239}Np \rightarrow {}^{239}Pu$$

Here, fissionable U-238 is converted into fissile Pu-239.

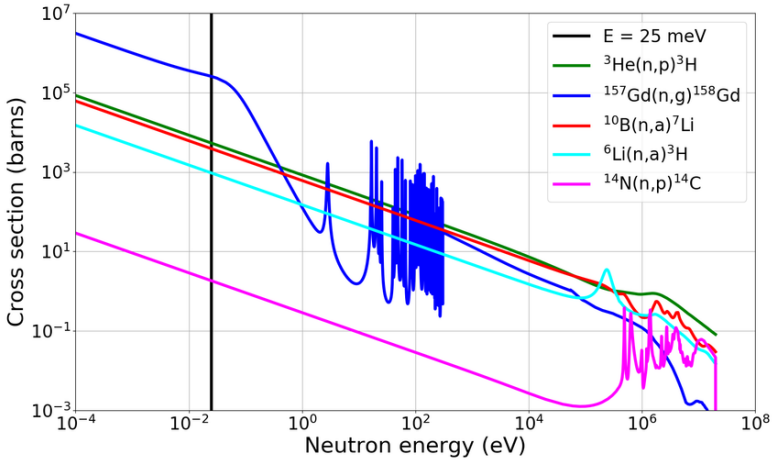

Figure 3.2: Capture cross section of the most commonly used neutron absorber [13]

Fission Fission is a nuclear process where heavy atomic nucleus splits in two, or more, lighter nuclei. This reaction is able to release a large amount of energy, as well as other particles such as neutrons, that play a key role in the whole process, since they are able to generate a fission chain.
Within the nucleus, the repulsive force between protons is balanced by the strong nuclear force. In big and heavy nuclei, this balance becomes fragile and in the right conditions, it can lead to the splitting of the atoms with a subsequent big release of energy. Usually nuclear fission happens when an atom absorbs a neutron, breaking the already tenuous balance, becoming unstable and splitting in two lighter nuclei. A standard nuclear fission reaction involving uranium-235 is:

$$^{235}\mathrm{U} + \mathrm{n} \rightarrow {}^{A}\mathrm{X} + {}^{A}\mathrm{Z} + \nu\,\mathrm{n} + \mathrm{Energy}$$

In this reaction uranium-235 absorbs a neutron, becomes unstable and splits into X and Z, ν neutrons and energy. ν is the neutron multiplicity factor, indicating the average number of neutrons produced per fission reaction. The usual values of ν for uranium-235 are:

Neutron Energy	Average ν (Neutrons per Fission)
Thermal neutrons	≈ 2.43
Fast neutrons	≈ 2.5–2.6
High-energy neutrons	Slightly higher (typically < 2.7)

Table 3.1: Average number of neutrons (ν) released per fission of ^{235}U, depending on the incident neutron energy.

The number of neutrons produced by a fission reaction is not fixed, since the reaction itself is a function of the energy of the projectile neutron and of the probabilistic nature of the event. As a matter of fact, fission is usually asymmetric, and the nucleus tends to split into 2 fission products (more rarely 3) with different masses. Indeed, multiple different reactions can take place, such as:

- $^{235}\mathrm{U} + \mathrm{n} \rightarrow {}^{95}\mathrm{Sr} + {}^{139}\mathrm{Xe} + 2\,\mathrm{n} + \mathrm{Energy}$
- $^{235}\mathrm{U} + \mathrm{n} \rightarrow {}^{90}\mathrm{Rb} + {}^{144}\mathrm{Cs} + 2\,\mathrm{n} + \mathrm{Energy}$

As with scattering and capture, the probability of such event is a function of the energy of the incident particle. In the case of Uranium-235, the lower the energy of the neutron, the higher the probability of having a fission. This strong bind can be seen in Figures 3.3 and 3.4:

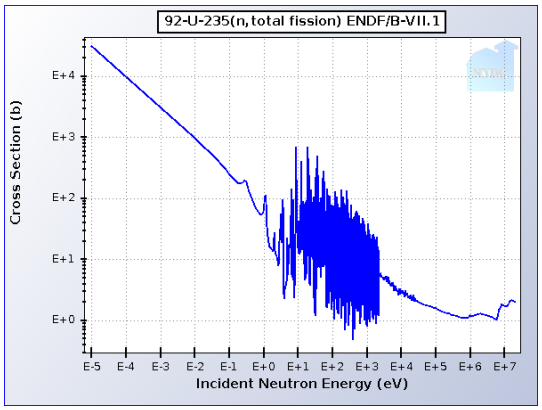

Figure 3.3: U-235 total fission cross section [14]

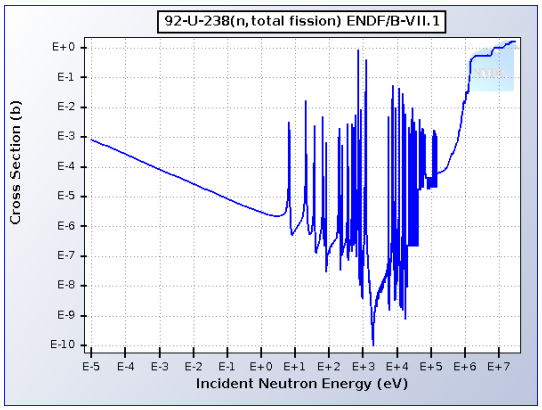

Figure 3.4: U-238 total fission cross section [14]

From Figures 3.3 and 3.4 we can really appreciate the huge difference in fission cross section between a fissile and a fissionable material.

The cross section spectrum of U-235 can be divided into 3 regions [15]:

- $1/v$ **Region:** this is the region in which the cross section is the highest because the nuclear force between the target nucleus and the neutron has more time to interact, due to the low velocity of the incident particle. The cross section value decreases with increasing energy of the neutron as 1/v
- **Resonance Region:** this is the region where many spikes appear. This happens because some neutrons have exactly the right energy to match certain energy levels in the nucleus. This match makes the probability of interacting much higher, leading to sudden spikes in the cross section spectrum. These particular energies have compound nuclei known as nuclear resonances.
- **Fast Neutron Region:** this is the region in which the cross section remains approximately constant

Particular attention must be paid to the risk of thermalisation in the U-238 capture cross section.

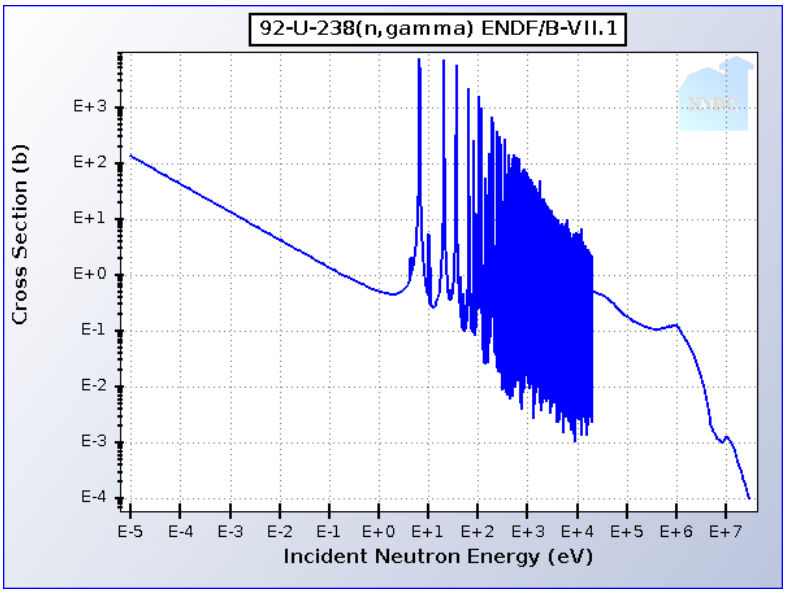

Figure 3.5: Capture cross section of U-238 [14]

As can be seen in Figure 3.5, the Σ_c of U-238 has resonance peaks in the range 2 eV - 24 keV, which can decrease the reactor efficiency by decreasing the number of neutrons available for fission. To decrease such effect, the moderator is usually kept physically separated from U-238.

3.1.2 Neutron multiplication factor evaluation

All these neutron interactions at the microscopic level, like absorption, scattering, and fission, add up to determine how the reactor behaves overall. This behavior is described by the neutron multiplication factor, k_{eff}, which tells us whether the reactor is subcritical, critical, or supercritical under certain conditions:

- $k_{eff} < 1$**:** the reactor is subcritical, meaning it won't be able to sustain a chain reaction because it is producing fewer neutrons than it consumes
- $k_{eff} = 1$**:** the reactor is critical meaning it produces exactly the same number of neutrons it consumes, so it is in a steady-state condition
- $k_{eff} > 1$**:** the reactor is supercritical. This is the condition in which a reactor works. The neutron population must be controlled to avoid an uncontrolled increase of power

There are different ways to derive k_{eff}. The ones analyzed here are the *Six factor formula* and the formula involving the geometrical buckling B^2.

Six factor formula The six factor formula [16]:

$$k = \eta \cdot f \cdot p \cdot \varepsilon \cdot P_f \cdot P_t \tag{3.3}$$

is composed by:

- η**: Neutron Reproduction Factor**. It is the number of neutrons produced per thermal neutron absorbed in the fuel:

$$\eta = \frac{\nu \cdot \Sigma_{f,\text{fuel}}}{\Sigma_{a,\text{fuel}}} \tag{3.4}$$

- **f: Fuel Utilization Factor**. It represents the fraction of neutrons absorbed by the fuel:

$$f = \frac{\Sigma_{a,\text{fuel}}}{\Sigma_{a,\text{fuel}} + \Sigma_{a,\text{mod}}} \tag{3.5}$$

- **p: Resonance Escape Probability**. It is the probability that a neutron will escape resonance capture, surviving and becoming a thermal neutron:

$$p = \frac{\text{Total number of thermal neutron}}{\text{Total number of fast neutrons}} \tag{3.6}$$

- ε**: Fast Fission factor**. It accounts for fast fissions that can happen before the neutrons have been slowed down. As we already talked about, fast fission will most likely happen in U-238 (fissionable material), since its fission cross section is higher at higher neutron velocity. Since its formula is:

$$\varepsilon = \frac{\text{Total neutrons from all fissions}}{\text{Neutrons from thermal fissions only}} \tag{3.7}$$

  its value is slightly higher than 1

- P_f**: Fast non-leakage probability**. It is the probability that a fast neutron, before being slowed down to thermal energies, will not leak out of the reactor core

- P_t**: Thermal non-leakage probability**. It is the probability that a thermal neutron will not leak out of the reactor core

Geometric buckling k_{eff} can also be evaluated introducing the concept of geometrical buckling:

$$k_{\text{eff}} = \frac{k_\infty}{1 + L^2 B^2} \tag{3.8}$$

where:

- k_∞ is the neutron multiplication factor in an infinite reactor

- B^2 is the geometric buckling that measures how the neutron flux changes shape in space due to the physical shape and size of the reactor

- L^2 that is the diffusion length squared, which represents the average path length of neutrons before being absorbed

For standard PWRs, in which the core geometry is typically cylindrical, the buckling correlation to be used is [17]:

$$B^2 = \left(\frac{2.405}{R}\right)^2 + \left(\frac{\pi}{H}\right)^2 \tag{3.9}$$

where H is the height of the reactor and R the radius. The higher these two parameters, the higher the k_{eff}, since there is a lower probability of neutrons escaping from the system.

Delayed neutrons To properly introduce the concept of reactivity, it is necessary firstly to explain the difference between prompt and delayed neutrons. Prompt neutrons are emitted immediately during the fission reaction and make up 99% of the total neutrons generated, while delayed neutrons are emitted milliseconds to minutes later by unstable fission products called precursors. The fraction of delayed neutrons β is the ratio between the number of delayed neutrons (i.e. neutrons emitted by fission product with some delay) and the total number of neutrons emitted by fission, while the fraction of effective delayed neutrons β_{eff} is the same ratio weighted for thermal energies. In thermal reactors, delayed neutrons are emitted at a lower energy than the prompt neutrons, 0.4 MeV against 2 MeV, so their leakage is less probable, but their contribution to fast fission is lower. These two effects tend to counterbalance each other and define the importance factor I. So β_{eff} can be expressed as the fraction of delayed neutrons β, weighted by their importance in sustaining the nuclear chain reaction [18]:

$$\beta_{eff} = \beta \cdot I \tag{3.10}$$

In reality, both the energy distribution and the importance of delayed neutrons vary from group to group (i.e. groups of fission products that decay), so β_{eff} can be rewritten as:

$$B_{\text{eff}} = \sum_{i=1}^{6} \beta_i \cdot \text{Importance}_i \tag{3.11}$$

where i runs over the delayed neutron groups.

Reactivity Reactivity is defined as:

$$\rho = \frac{k_{eff} - 1}{k_{eff}} \tag{3.12}$$

therefore it is directly linked to the neutron multiplication factor. While k_{eff} provides a direct measure of neutron population behaviour, the offset from criticality is quantified by the reactivity ρ. In fact, if $k_{eff} < 1$, then $\rho < 0$, if $k_{eff} = 1$, then $\rho = 0$ and if $k_{eff} > 1$, then $\rho > 0$. Reactivity is dimensionless but is usually expressed in per cent mille (pcm), where 1 $pcm = 10^{-5}$ or in dollars, depending on the fraction of effective delayed neutrons β_{eff}. Reactivity is tightly linked to delayed neutrons because they contribute to a slower response of the reactor after a change in reactivity.

3.1.3 Neutron flux and neutron current

Neutron flux Due to the high density of neutrons in a reactor or medium, their behavior is described using the neutron flux. Unlike other physical fluxes, which

might describe particles simply passing through a surface, the neutron flux is defined as the total distance traveled by all neutrons per second, per unit volume, with units of $\frac{\text{neutrons}}{cm^2 \cdot s}$. Due to the wide range of neutron energies, the neutron flux is typically expressed as a function of energy. This results in the neutron flux spectrum, which shows how the flux is distributed across different energies.

$$\phi(\vec{r}, E, \vec{\Omega}, t) = v(E) \cdot n(\vec{r}, E, \vec{\Omega}, t) \tag{3.13}$$

Equation (3.13) is the general expression for neutron flux. $v(E)$ is the neutron speed as a function of energy, while $n(\vec{r}, E, \vec{\Omega}, t)$ is the angular neutron density. The neutron flux depends on the following variables: position of the neutrons $\vec{r}$, their energy E, their travelling direction $\vec{\Omega}$ and the time t.

Neutron current While neutron flux tells us how many neutrons are moving around in a material overall, neutron current gives us the net flow of neutrons in a particular direction. Flux includes all neutrons, no matter which way they're going, while current reflects the net difference between neutrons moving in opposite directions.
Even though both have the same units $\frac{\text{neutrons}}{cm^2 \cdot s}$, there is an important distinction: neutron current is a vector, meaning it has both size and direction, making it especially important when studying neutron behaviour near reactor boundaries.

3.2 General overview of the Monte Carlo method

The Monte Carlo (MC) method is a statistical technique used to simulate mathematical or physical experiments computationally. In engineering, it is particularly suited for modeling complex systems composed of random processes governed by known or assumed probability density functions [19]. It relies on repeated random sampling to solve deterministic problems, introducing an unavoidable uncertainty that must be carefully taken into account. The main characteristics of the method are:

- **Random sampling:** the MC method is based on the generation of random sample, ψ, following a probability distribution that should represent as much as possible the problem under investigation

- **Probability distribution:** the output of a MC simulation strongly depends on the distribution chosen. The most common distributions are uniform, normal, exponential and poissonian

- **Law of Large Numbers:** as the number of sample increases, the solution becomes more and more precise and realistic, decreasing the uncertainty related to it.

The flow of thoughts of the application of a MC code can be summarized as:

1. **Statistical phenomenon:** choice of the statistical phenomenon to study
2. **Outcome variable:** association of a variable to the outcome of such statistical phenomenon
3. **Performing of the experiment**
4. **Random sample:** association of the random variable ψ_i to each outcome
5. **Sample average:** evaluation of the sample average
6. **Variance:** evaluation of the variance and of the mean standard deviation

The sample average is the single number that contains all the outcomes of the experiments (ψ_i):

$$\psi^{(n)} = \frac{1}{N} \cdot \sum_{i=1}^{N} \psi_i \tag{3.14}$$

Being the container of all the random outcomes of each the experiment, it is a random value as well.
Instead, the variance is a key parameters that express the level of dispersion of the results obtained during the repeated random sampling. Obviously, this value should be as low as possible to have the best result possible. The variance of the sample average is:

$$\sigma^2[\psi^{(n)}] = \frac{\sigma^2[x]}{N} \tag{3.15}$$

As can be seen, the higher the number of samples (i.e. of experiments), the lower the dispersion of the results, and the higher the precision.
The mean standard deviation is simply the square root of the variance of the sample average:

$$\sigma[\psi^{(n)}] = \sqrt{\sigma^2[\psi^{(n)}]} = \frac{\sigma[x]}{\sqrt{N}} \tag{3.16}$$

The result of a MC estimation is typically expressed as the sample average accompanied by its mean standard deviation:

$$\text{Result} = \psi^{(n)} \pm k \cdot \sigma \left[\psi^{(n)}\right] \tag{3.17}$$

From Equations 3.16 and 3.17, it can be observed that the uncertainty related to the result decreases slowly with increasing sample size N, as it is inversely proportional to the square root of N.
According to the ***Central Limit Theorem***, as $N \to \infty$, the distribution of the sample average approaches a normal (Gaussian) distribution, regardless of the distribution of the individual samples. This justifies the use of confidence intervals to express the uncertainty in the result and gives meaning to the parameter k in Equation 3.17.
The value of k determines the confidence level, i.e. the probability that the true mean lies within the given error bounds:

- $k = 1$ corresponds to a confidence level of approximately 68%
- $k = 2$ corresponds to a confidence level of approximately 95%
- $k = 3$ corresponds to a confidence level of approximately 99%

Even though the edges of an MC estimation are multiple, such as:

- handle of complex problems whose analytical solutions are difficult or impossible
- be able to model systems with random or non-linear behaviour
- easy to implement for many applications
- works well for sensitivity analysis and risk assessment

it has some disadvantages to take into account:

- slow convergence due to the error decreasing as the $1/\sqrt{N}$
- computationally expensive for large simulations
- results are statistical, so are always accompanied by an uncertainty

3.3 TRIPOLI-5 Code Overview

The Monte Carlo (MC) method is the foundation of TRIPOLI-5 (T-5) [20], the under development code carried out by SERMA at CEA and SNC at IRSN. It is a continuous-energy neutron transport MC code, able to simulate fixed sources and criticality problems in steady-state. In this study, TRIPOLI-5 was used to simulate the Small Nuclear Reactor Engine, described in detail in Subsection 2.4 of Chapter **??**. In the context of nuclear applications, the statistical process being modeled is the movement and interaction of neutrons inside the reactor core.
In Monte Carlo particle transport simulations, a score is a calculated quantity that provides insight into particle behavior, such as flux, reaction rates, k-effective, and other transport characteristics [20]. Among them, the most used during the internship were the k score, which evaluates the neutron multiplication factor k 3.1.2, the reaction rates score and the flux score. In particular, the latter is able to evaluate the flux spectrum for each volume in the geometry using the collision estimator, on a given energy discretization mesh.
The equation that is able to describe such behaviour is the neutron transport equation:

$$\begin{aligned}\frac{1}{v(E)}\frac{\partial\psi(\vec{r},\vec{\Omega},E,t)}{\partial t} + \vec{\Omega}\cdot\nabla\psi(\vec{r},\vec{\Omega},E,t) + \Sigma_t(\vec{r},E)\psi(\vec{r},\vec{\Omega},E,t) = \\ = \int\int \Sigma_s(\vec{r},E'\to E,\vec{\Omega}'\cdot\vec{\Omega})\psi(\vec{r},\vec{\Omega}',E',t)\,dE'\,d\Omega' + \\ + \frac{\chi_p(\vec{r},E)}{4\pi}\int\int(1-\beta)\nu_p(E')\Sigma_f(\vec{r},E')\psi(\vec{r},E',\vec{\Omega}',t)\,dE'\,d\Omega' \\ + \sum_{i=1}^{G}\frac{\chi_{d,i}(\vec{r},E)}{4\pi}\lambda_i C_i(\vec{r},t) + S(\vec{r},\vec{\Omega},E,t) \quad (3.18)\end{aligned}$$

Let's break it down to study the single terms:

Left side of the equation

- $\frac{1}{v(E)}\frac{\partial\psi(\vec{r},\vec{\Omega},E,t)}{\partial t}$ describes the time rate change of the neutron angular flux
- $\vec{\Omega}\cdot\nabla\psi(\vec{r},\vec{\Omega},E,t)$ represents the neutrons moving through space without interactions (i.e. on straight paths)
- $\Sigma_t(\vec{r},E)\psi(\vec{r},\vec{\Omega},E,t)$ is the total removal term which represents the loss of neutrons due to fission, scattering and capture

Right side of the equation All the terms in the right side of the equation represents a gain of neutrons, that can be due to scattering, fission or an external source:

- $\int\int \Sigma_s(\vec{r}, E' \rightarrow E, \vec{\Omega}' \cdot \vec{\Omega})\psi(\vec{r}, \vec{\Omega}', E', t)\, dE'\, d\Omega'$ represents the neutrons that from their original state, Energy = E' and direction = Ω', has been scattered in Energy = E and direction = Ω, so there is a gain of neutrons
- $\frac{\chi(\vec{r},E)}{4\pi} \int\int (1-\beta)\nu_p(E')\Sigma_f(\vec{r}, E')\psi(\vec{r}, E', \vec{\Omega}', t)\, dE'\, d\Omega'$ describes the gain of neutrons from fission. $\chi(E)$ is the energy spectrum of the emitted neutrons
- $\sum_{i=1}^{G} \frac{\chi_{d,i}(\vec{r},E)}{4\pi}\lambda_i C_i(\vec{r}, t)$ represents the delayed neutron source term. While prompt neutrons are emitted immediately during fission, delayed neutrons are emitted later by the radioactive decay of unstable fission products, called precursors.
- $S(\vec{r}, \vec{\Omega}, E, t)$ represents an external neutron source

Delayed neutrons come from delayed neutron precursors which change overtime and, therefore, need a time dependent equation describing their evolution:

$$\frac{\partial C_i(\vec{r}, t)}{\partial t} = \beta_i \int\int \nu(\vec{r}, E)\Sigma_f(\vec{r}, E)\psi(\vec{r}, E', \vec{\Omega}', t)\, dE'\, d\Omega' - \lambda_i C_i(\vec{r}, t), \qquad i = 1, \ldots, G \tag{3.19}$$

Let's now analyze the precursor equation associated with delayed neutrons:

Terms of the precursor equation

- $\frac{\partial C_i(\vec{r},t)}{\partial t}$ describes the time variation of the concentration of delayed neutron precursors belonging to group i
- $\beta_i \int \nu(\vec{r}, E)\Sigma_f(\vec{r}, E)\psi(\vec{r}, E', \Omega', t)\, dE'\, d\Omega'$ represents the production term of precursor nuclei. It is proportional to the fission rate and to the delayed neutron fraction β_i associated with precursor group i
- $\lambda_i C_i(\vec{r}, t)$ is the loss term due to the radioactive decay of precursor nuclei. This decay is responsible for the emission of delayed neutrons

To characterize the flight of a neutron, and subsequently solve the neutron transport equation 3.18, it is useful to introduce the concept of Random Walk (RW). A RW represents the stochastic process governing a neutron's behavior throughout its lifetime. It is characterized by its initiation, followed by free flight, changes in direction and position due to scattering, and its termination, which occurs either through fission, absorption, or leakage from the reactor boundary.

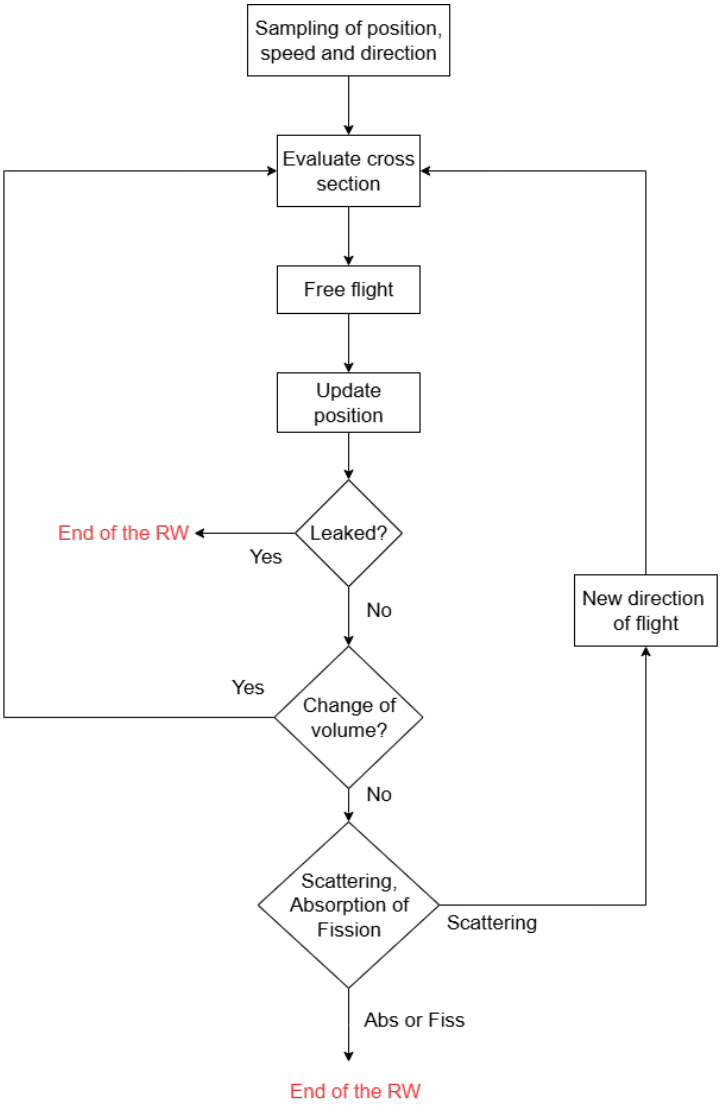

Figure 3.6: Flow chart of the RW of a neutron

From the random walk it becomes possible to estimate key physical quantities, such as neutron flux, reaction rates, and how neutrons are distributed in space and energy, providing insight into how the reactor behaves. This is the basic approach used during the development of TRIPOLI-5. The source of the neutron can be either a point source, an uniform plane source or radiative heat coming from a surface, while the direction of emission can be isotropic, a collimated source or it can follow Lambert's law. During the implementation of the phenomenon studied in this report, an isotropic point source has been used. The law of the free flight is the exponential:

$$f(s)ds = \Sigma \cdot e^{-\Sigma s} \tag{3.20}$$

3.3.1 T5 geometry definition

The TRIPOLI-5 geometries are made using its the AGORA geometry module. The flow of thoughts of the creation of a geometry is the following [20]:

Region → Shape → Volume → Universe → Geometry

where:

- *Regions* are single elementary surfaces such as planes and cylinders
- *Shapes* are a combinations of Boolean operators (intersection, union or component) and half-spaces, which are defined with respect to regions
- *Volumes* are Shapes associated with a material
- *Universes* are containers that group volumes or composite structures, allowing for modular geometry construction
- *Geometries* are the final object used to run the simulation, in this case the SNRE core and surrounding components

Tie tube element In the first place tie tube was built, mainly thanks to the Z-Cylinder class of the AGORA module:

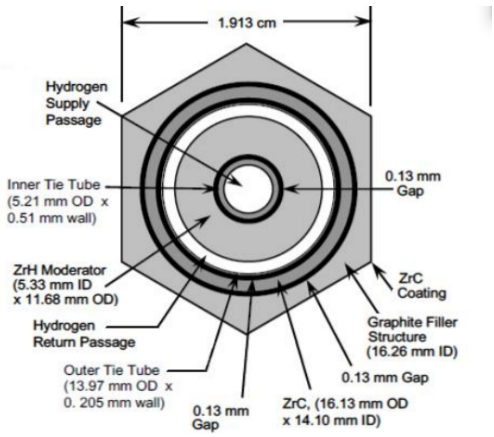

Figure 3.7: Tie tube element [8]

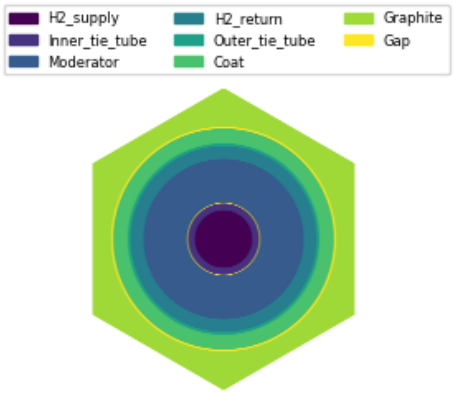

Figure 3.8: T-5 tie tube geometry

Fuel element Next up is the fuel element. Its geometry was built by exploiting different kind of regions and shapes, including custom planes (that satisfy $ax + by + cz = d$ equation), Z-Cylinders and Hexagonal lattice feature, needed to place more easily the holes where the hydrogen passes:

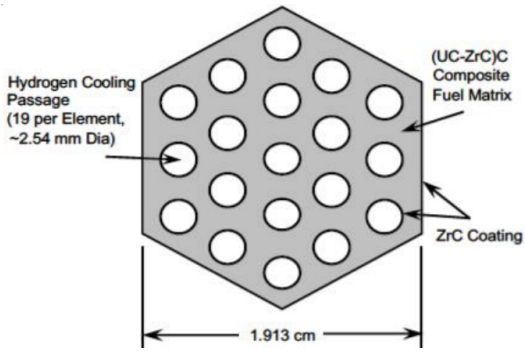

Figure 3.9: Fuel element [8]

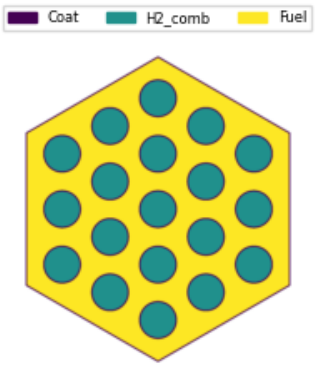

Figure 3.10: T-5 fuel element geometry

Core, Reflector assembly and Vessel The universes built for the two elements above have been utilized for the construction of the core. As mentioned in Subsection 2.4, the core is composed by 805 elements, 564 of fuel and 241 of tie tubes. These are arranged in a hexagonal lattice, where each cell is filled with its predefined universe, corresponding to either a fuel element or a tie tube.
In order to have each tie tube surrounded by fuel elements, a small algorithm has been implemented, in which two indexes identify the position in the lattice:

- **j:** that identifies the diagonal coordinate
- **i:** that identifies the horizontal coordinate

The small algorithm replaces some lattice elements with the tie tube universe previously built:

Algorithm 1 Tie tubes placement in the Lattice Geometry Population

```
1: for j ← min_range_value to max_range_value − 1 do
2:     for i ← min_range_value to max_range_value − 1 do
3:         if |i + j| < max_range_value then
4:             if    (j is even and (i − j) mod 3 = 0) or
                     (j is odd and (i − (j − 3)) mod 3 = 0)
   then
5:                 Set geom_lattice(i, j, 0) ← tie_tubes_universe
6:                 Increment nb_tie_tubes by 1
7:             end if
8:         end if
9:     end for
10: end for
```

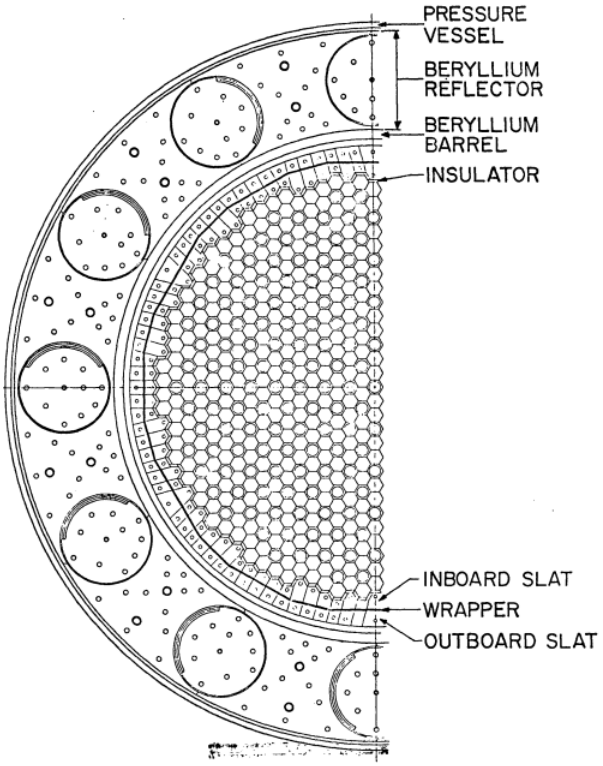

Figure 3.11: Transverse section of the reactor [8]

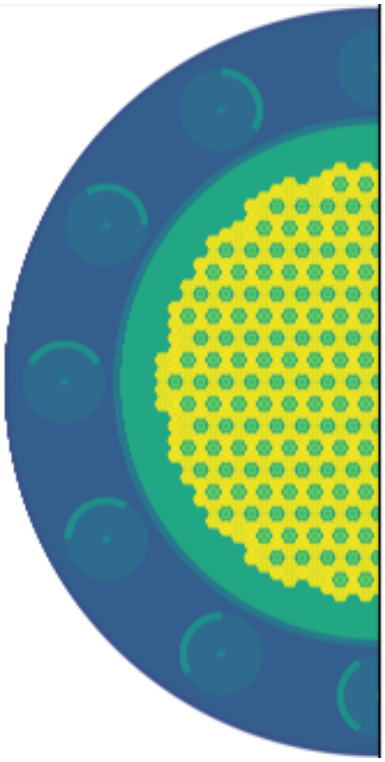

Figure 3.12: T-5 transverse section of the reactor

Since not all the reactor core is filled with fuel or structural elements, the remaining space must be occupied by graphite, which will act as moderator. To do so, a small algorithm has been carried out. Its goal is the replacement of any tie tubes or fuel elements whose center lies at a distance from the core center greater than *core_radius*:

Algorithm 2 Lattice Geometry Population Based on Distance

for $j \leftarrow$ min_range_value to max_range_value $- 1$ **do**
  for $i \leftarrow$ min_range_value to max_range_value $- 1$ **do**
    if $|i + j| <$ max_range_value **then**
      if $i = 0$ **then**
        $distance\_cells \leftarrow hexagon\_pitch \cdot |j|$
      else if $j = 0$ **then**
        $distance\_cells \leftarrow hexagon\_pitch \cdot |i|$
      else if $i \cdot j > 0$ **then**
        $distance\_cells \leftarrow hexagon\_pitch \cdot \sqrt{i^2 + j^2 - 2ij \cdot \cos\left(\frac{2\pi}{3}\right)}$
      else
        $distance\_cells \leftarrow hexagon\_pitch \cdot \sqrt{i^2 + j^2 + 2ij \cdot \cos\left(\frac{\pi}{3}\right)}$
      end if
      if $distance\_cells \geq core\_radius$ **then**
        $geom\_lattice[i, j, 0] \leftarrow graphite\_universe$
        $count\_cell \leftarrow count\_cell - 1$
        if $(j \bmod 2 = 0$ **and** $(i - j) \bmod 3 = 0)$ **or**
          $(j + 1 \bmod 2 = 0$ **and** $(i - (j - 3)) \bmod 3 = 0)$
        then
          $nb\_tie\_tubes \leftarrow nb\_tie\_tubes - 1$
        end if
      end if
      if $distance\_cells \geq core\_radius - hexagon\_pitch$ **and**
        $geom\_lattice[i, j, 0] \leftarrow tie\_tube\_universe$
      then
        $geom\_lattice[i, j, 0] \leftarrow fuel\_element\_universe$
        $nb\_tie\_tubes \leftarrow nb\_tie\_tubes - 1$
      end if
    end if
  end for
end for

Outside the core we can find a thin layer of beryllium barrel, the reflector and the vessel. Inside the reflector assembly there are 12 drums and 12 control plates.

As shown in Figure 3.13, different layers of materials are visible on top of the reactor. From top to bottom, there is a tungsten layer, followed by a lithium layer (used as a reflector), and an aluminum layer sandwiched between two thin hydrogen layers. At the bottom, the hydrogen flow exiting through the nozzle can be observed.

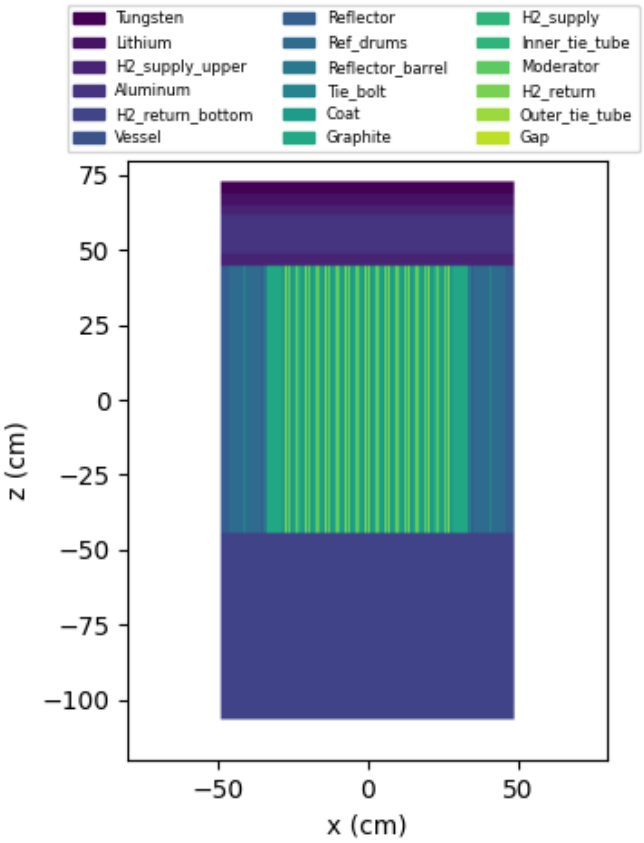

Figure 3.13: Axial section of the reactor

T5 physics configuration The physics configuration includes both the medium builder and the source definition. In this study:

- **Medium:** it was built starting from a catalog of nuclide loaded from the Evaluated Nuclear Data File (ENDF) thanks to the DELOS API

- **Source:** it is a point isotropic source with center in the origin of the xyz *axis*, whose particle type is *Neutrons* and energy distribution *Monokinetic* at 2 MeV. In the source builder also some features of the CORE API have been used such as the *ParticleType* and *Point* modules

The exact material compositions can be found in the Annex 8.2. The concentrations of isotopes are given in $atom/(cm \cdot barn)$ since it is how MENDEL evaluates them.

3.3.2 T5 standalone results

Figure 3.14 shows the neutron flux per unit lethargy in the whole geometry. The fission reaction generally produces neutrons at 2 MeV of energy, so as they begin to slow down, the peak tends to be in the vicinity of 1.5 MeV. The presence of two peaks at low energies may be related to the fact that the flux is integrated over the whole geometry. Different regions, such as the moderator and the reflector, may contribute with thermal peaks at different energies, and their superposition can therefore produce a double-peaked structure in the global spectrum.

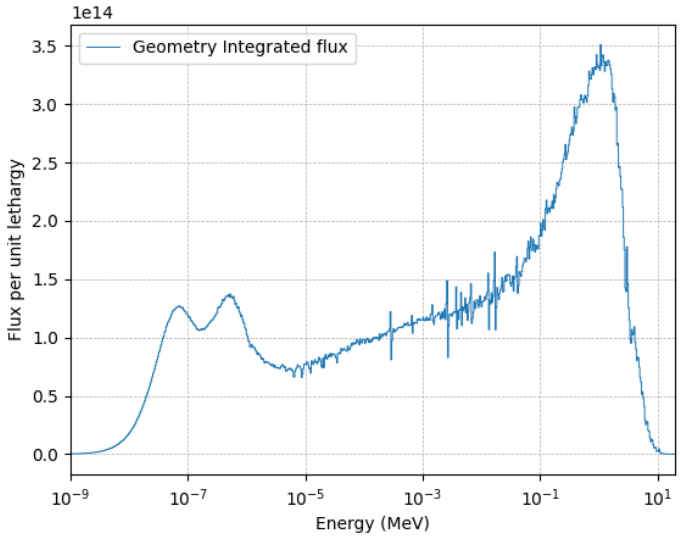

Figure 3.14: Flux per unit lethargy in the whole geometry

As better explained in Chapter 4, the core has been divided into five concentric rings, to better analyze the behaviour of the NTP reactor and to catch the different depletion across different regions of the core. The following figures show the key parameters, such as the neutron flux and the reaction rates, within each of the defined rings.

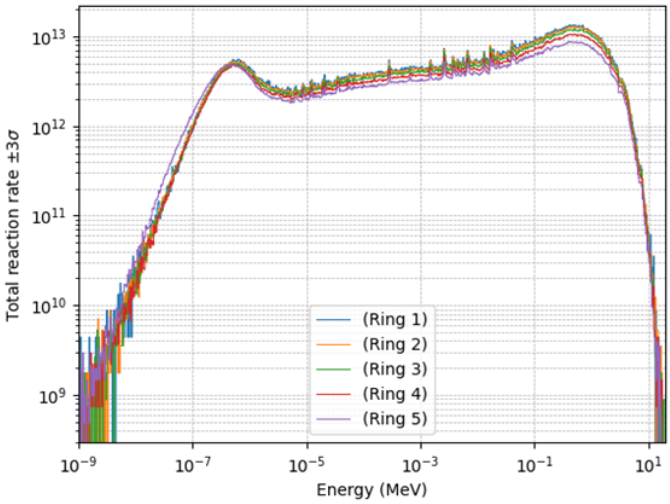

Figure 3.15: Total reaction rate in each ring

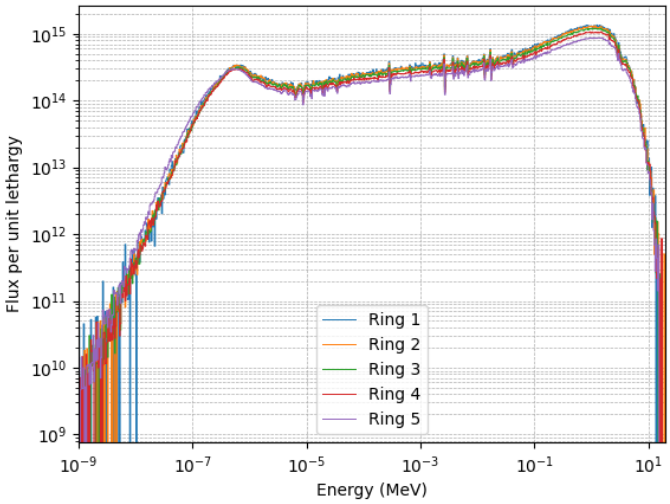

Figure 3.16: Flux per unit lethargy in each fuel ring

Figures 3.15 and 3.16 show two classical outputs from the T-5 estimation: the flux score of the fuel and the total reaction rate score. As observed, both the flux and the total reaction rate reach their maximum around 1.5 MeV.
As expected the first ring, located at the center of the core, exhibits the highest neutron flux and corresponding reaction rates for most of the energy spectrum.

This central dominance is even more pronounced than it seems fro the figures, as the y-axis limits compress the scale and partially mask the magnitude of the flux difference. At lower energies, however, an inversion of this trend is observed, with the outer rings showing relatively higher reaction rates. This behavior can be attributed to the presence of the reflector surrounding the core. Made of beryllium, which also acts as a moderate neutron moderator, the reflector slows down fast neutrons that escape the core, increasing the thermal neutron population in the outer regions. As a result, low-energy reaction rates are higher near the periphery.

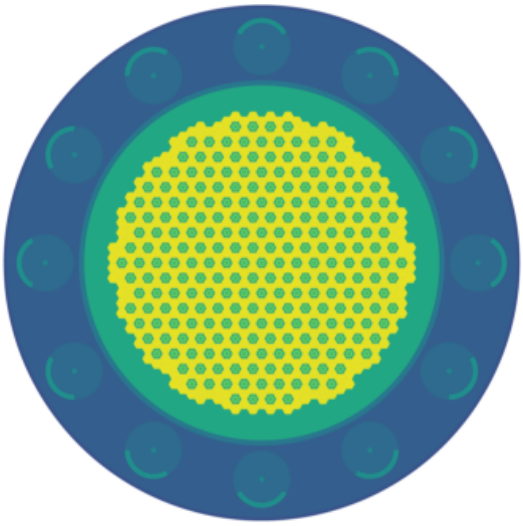

Figure 3.17: Control plate configuration corresponding to the maximum neutron multiplication factor, k

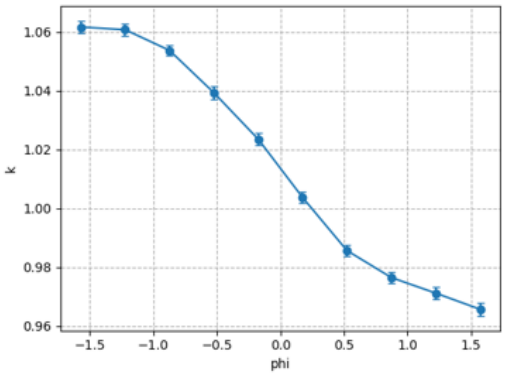

Figure 3.18: Neutron multiplication factor (k) as a function of control plate tilt angle (in radians) at 2500 K

Another noteworthy result is illustrated in Figure 3.18, which shows the strong influence of the control plates tilting angle on k. The initial angle is the one in Figure 3.17, representing the position where the control plates are the furthest and therefore the neutron multiplication factor is the highest.
By examining Figure 3.18, it can be inferred that the reactor's criticality can be fully regulated, either brought into a subcritical or supercritical state, solely by adjusting the tilt angle of the control plates. Notably, achieving criticality ($k = 1$) corresponds to a control plate tilt angle of approximately 0.2 to 0.25 radians.

4 | MENDEL Depletion Code

This chapter presents the basics of the depletion mechanism of materials under neutron irradiation, along with the MENDEL implementation of all the materials depletion inside the SNRE. Some MENDEL outputs will be provided and commented.

4.1 General overview of the depletion

4.1.1 Depletion mechanisms

In the nuclear field, the depletion mechanism is a key aspect to take into account and it is related to the change of a material due to the irradiation by neutrons over time. During the operation of a nuclear reactor, the fuel becomes gradually depleted due to the interaction of its nuclei with neutrons. These continuous reaction results in the progressive reduction of the initial fissile material concentration in the fuel and consequently to the decrease of the rate of nuclear fission reaction in the core over time, leading to the reduction of the effective multiplication factor k.

Fission products One of the primary consequences of fuel depletion is the buildup of fission products, generated during fission, that often possess high neutron absorption cross section, decreasing even more the reactivity [21]. This reduction directly correlates with the energy extracted from the fuel and is often quantified in terms of burnup, usually expressed in gigawatt-days per metric ton of heavy metal, GWd/MTU or megawatt-days per kilogram, MWd/kg. The neutron flux spectrum, power distribution and irradiation time play a huge role in computing these calculations, as they strongly affect the rate at which fissile isotopes are consumed and new isotopes are produced.

Neutron capture Due to neutron capture reactions and subsequent beta decay (further explained below), Transuranic elements are generated (also called minor actinides). Transuranic elements are those heavier than uranium (i.e. atomic mass > 92) and are usually produced by the neutron capture from a fertile element

such as U-238. This reaction has a high probability of happening due to their big capture cross section at thermal energies as well as some really high peaks in the epithermal energy region (due to resonances) as better explained in Paragraph 3.1.1.

Decay The decay reaction is a mechanism that happens when a nucleus is unstable and cannot maintain its current configuration, losing energy by radiation. The most common decays processes are [22]:

- **Beta Decay β^-:** in which a neutron inside the nucleus transforms into a proton by the emission of an electron and an antineutrino

$$n \rightarrow p + e^- + \bar{\nu}_e$$

$$^{14}_{6}\mathrm{C} \rightarrow ^{14}_{7}\mathrm{N} + e^- + \bar{\nu}_e$$

- **Alpha Decay α:** in which a an unstable nucleus emits an alpha particle, consisting of two protons and two neutrons. This particle is actually a helium-4 nucleus. A classical example in nuclear fission reactors is:

$$^{238}_{92}\mathrm{U} \rightarrow ^{234}_{90}\mathrm{Th} + ^{4}_{2}\mathrm{He}$$

  in which Uranium-238 decays alpha, generating a Thorium-234 nucleus and an helium-4 nucleus

- **Gamma decay γ:** which is distinguished from other nuclear decay modes by the fact that it does not involve a transformation in the chemical identity or composition of the nucleus. Specifically, the process entails the emission of a high energy gamma photon, electrically neutral radiation. As a result, both the atomic number and the mass number of the nucleus remain unchanged. Gamma decay typically follows an α or β^- decay, which leaves the daughter nucleus in an excited energy state. The emission of a gamma photon facilitates the de-excitation of the nucleus, allowing it to transition from a higher to a lower energy level without altering its proton or neutron count. An example:

$$^{60}_{28}\mathrm{Ni}^* \rightarrow ^{60}_{28}\mathrm{Ni} + \gamma$$

Figure 4.1 exhibits the U-238 decay chain, composed by several α and β^- decays. The series terminates with the stable Lead-206 isotope.

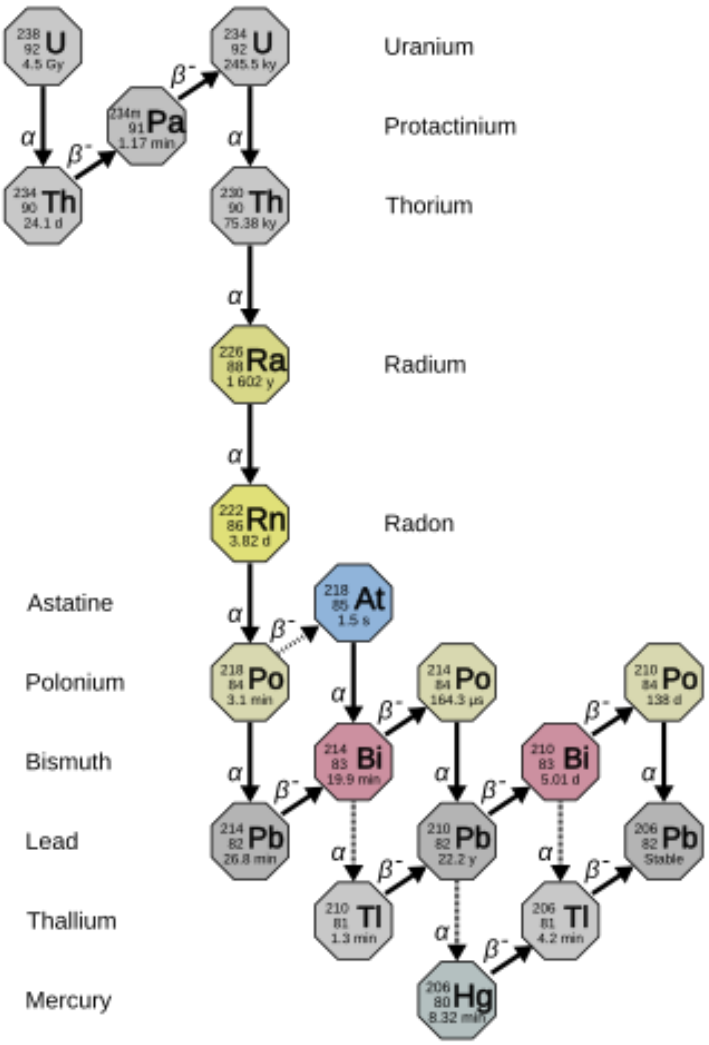

Figure 4.1: U-238 decay chain [23]

4.1.2 Half-life

In general the time needed by a radioisotope to undergo radioactive decay varies greatly depending on the isotope, because each radioisotope has a unique nuclear

structure, which determines how unstable it is. This instability affects how fast it decays and it is measure by the half-life. The half-life is the time needed for half the nuclide to decay in the sample under observation. This value can range from milliseconds to billion of years and it is directly related to the decay constant λ, that is the probability per unit time that a nucleus will decay:

$$T_{1/2} = \frac{ln(2)}{\lambda} \tag{4.1}$$

Isotopes with similar decay constants are often grouped together because it makes it easier to predict how they behave over time and to model their decay chains more effectively. This approach is useful in applications where understanding the timing and sequence of radioactive transformations is important. The mathematical foundation for such modeling is provided by the Bateman equations, which describe the time-dependent activity of each member in a decay chain based on their respective decay constants.

Bateman equation The Bateman equation provides the mathematical framework to quantify the time-dependent evolution of nuclide concentrations in a radioactive decay chain or under neutron irradiation. The simplest case possible is the two-nuclide decay chain, with N as number of nuclei [24]:

$$\begin{cases} \dfrac{dN_1}{dt} = -\lambda_1 N_1 \\ \dfrac{dN_2}{dt} = \lambda_1 N_1 - \lambda_2 N_2 \end{cases} \tag{4.2}$$

The system presented in Equation 4.2 illustrates the radioactive decay of the parent isotope (isotope 1) and the consequent formation of the daughter isotope (isotope 2). It is evident that the daughter isotope is also unstable and undergoes radioactive decay characterized by a different decay constant, denoted as λ_2. In this context, the product λN is commonly referred to as the activity A.

More in general, to account for different reaction chains and neutron irradiation induced mechanisms, the Bateman equation is extended to include terms representing neutron-induced transmutations such as neutron capture and fission:

$$\frac{dN_i(t)}{dt} = \sum_j \sigma_{j\to i}\,\phi(t)\,N_j(t) + \sum_k \lambda_k\,b_{k\to i}\,N_k(t) - \sigma_i\,\phi(t)\,N_i(t) - \lambda_i N_i(t) \quad (4.3)$$

Left part of the equation The left-hand side of the equation is only composed by the derivative of N_i that is the rate of change in the number of nuclide i

Right part of the equation The right-hand side of the equation comprehends the processes that govern the time-dependent behaviour of the nuclide. Terms with the plus sign in front contribute to the production of the nuclide. On the other hand, terms with a negative sign represent processes that lead to its depletion:

- The first term $\sum_j \sigma_{j\to i}\,\phi(t)\,N_j(t)$ represents the nuclear reactions that produce the nuclide i under consideration. These reactions may include both neutron-induced fission and neutron capture processes, depending on the isotope j and on the microscopic cross-section associated with the transformation $\sigma_{j\to i}$. The j index runs on all the kind of isotopes able to transmute into isotope i
- The second term $\sum_k \lambda_k\,b_{k\to i}\,N_k(t)$ accounts for the decay process of a general nuclide k into the nuclide i. Here, $b_{k\to i}$ is the branching ratio and it represents the probability that a radioactive nuclide will decay into a specific daughter nuclide i among several possible decay paths
- The third term $\sigma_i\,\phi(t)\,N_i(t)$ is subtractive in nature, since it removes a i nuclide when this undergoes fission or capture
- The last term $\lambda_i N_i(t)$ represents the decay process of the isotope i, decreasing the amount of its nuclides

4.2 MENDEL code

4.2.1 MENDEL solvers and material depletion

Considering all isotopes of every element and accounting for the full range of nuclear reactions and decay processes that can take place, the Bateman Equation 4.3 can become really complex and analytically intractable. For this reason numerical

solvers have been developed to facilitate the practical solution of such system. Various numerical integration methods have been implemented, including those incorporated in the MENDEL depletion code. Among the most notable are the 4th-order Runge-Kutta method (RK) and the Chebyshev Rational Approximation Method (CRAM), which is particularly well-suited for solving large ordinary differential equations systems. Let's dig some more inside these 2 solvers. The Bateman Equation 4.3 can be written in matrix form as:

$$\begin{cases} \dfrac{dN}{dt}(t) = A(t)N(t) \\ N(0) = N_0 \end{cases} \tag{4.4}$$

Runge-Kutta method In MENDEL matrix $A(t)$ can be considered constant, linear or quadratic in time [25]. Due to the constraint given by the Courant-Friedrichs-Lewy (CFL) condition for convergence, the time steps of the calculation will be too small. That's why in the 4th-order RK the nuclides are split in saturated and non-saturated ones (that means that their concentration still heavily changes in time and therefore they haven't reached equilibrium yet).

CRAM method The CRAM method utilizes the assumption of $A(t) = A$, meaning that matrix exponential method can used, exploiting the Incomplete Partial Fraction method (IPF). CRAM works by approximating a function using a fraction, where both the numerator and denominator are polynomials [25]:

$$\exp(A\Delta t) = \alpha_0 \prod_{l=1}^{k/2} \left(I + 2\,\Re\left[\alpha_l (A\Delta t - \theta_l I)^{-1}\right]\right) \tag{4.5}$$

The accuracy of the CRAM method is roughly 10^{-n} with n that is the CRAM method order (set at 48 for this report's computations). The CRAM solver has been chosen for its lower computation time with the increasing number of non-saturated nuclides. This numerical approach enables MENDEL to accurately model complex transmutation chains while maintaining computational efficiency. However, the accuracy of MENDEL's calculations critically depends on the data inputs. MENDEL takes as outside data:

- A list of isotopes and nuclear reactions (decay and induced by neutrons) between those isotopes, with their corresponding cross sections
- A list of fission yields in nuclear libraries

- Some libraries of nuclear data to compute the decay heat, the activity and the emission spectrum

In this work I developed a modular interface, able to run just by giving it as input:

1. The depletion chain path and the fission yields path
2. The energy mesh, which discretizes the energy spectrum, that is defined based on the previously specified path and consists of 281 bins in this case
3. The actual flux exchanged from TRIPOLI-5 to MENDEL, subdivided in 281 bins as well
4. The materials list to deplete

The general workflow adopted is as follows:

Algorithm 3 MENDEL Workflow with Multiple Materials

```
SetSolver(solver_type, paths)
GetFluxFromTripoli5(flux_data)
for each material in materials do
    SetInitialConcentrations(material)
    new_concentration ← EvaluateConcentrationWithCRAM(material)
    UpdateConcentrations(material, new_concentration)
end for
SetConcentrationsInTripoli5(new_concentration)
```

As can be seen in the Algorithm 3, the MENDEL code implementation allows for the simultaneous depletion of multiple materials. The main limitation of the current implementation lies in the use of a single, shared depletion chain for all materials. As a result, even non-fissile materials are processed using the same complex depletion chain and fission yield data as fissile materials, which can lead to increased computational cost without really improving the accuracy of the results.

4.2.2 MENDEL standalone results

Concentration computation

MENDEL consists of a deterministic component and a stochastic component. The latter is used only when the objective is to evaluate and propagate uncertainties. Since the following results do not include uncertainty analysis, only the deterministic part of MENDEL was used. To better analyze the behavior of the NTP reactor

engine, the core has been divided into five concentric rings, allowing for the assessment of fuel depletion variations across different regions of the core as a function of distance from the center. The following results include the standalone evaluation of the concentrations (in $atom/(cm \cdot barn) \cdot 10^{24}$) of the seven most common fission products of U-235, along with the concentrations of Pu-239, U-235 and U-238 at various time intervals, in the outermost core ring:

Isotopes	**0h**	**2h**	**14h**
Iodine-131	0.0	9.867e-09	1.323e-07
Cesium-137	0.0	4.903e-08	3.566e-07
Strontium-90	0.0	4.534e-08	3.280e-07
Xenon-135	0.0	3.660e-09	2.115e-08
Krypton-85	0.0	3.567e-10	9.871e-09
Barium-140	0.0	5.142e-08	3.579e-07
Zirconium-95	0.0	4.940e-08	3.844e-07
Uranium-235	7.977e-04	7.966e-04	7.902e-04
Uranium-238	5.476e-05	5.474e-05	5.463e-05
Plutonium-239	0.0	1.325e-10	9.537e-09

Table 4.1: Isotopes concentrations at $t = 0\ h$, and after 2 and after 14 hours

From Table 4.1 above, it can be observed that the fuel is undergoing proper depletion: the concentrations of the fission products (first seven nuclides) and plutonium isotopes are increasing, while the concentrations of U-235 and U-238 are decreasing, indicating the expected fuel burnup behaviour.

To further emphasize the proper depletion of the fuel, in the following plots it can be observed some of the fission products concentrations changing over a 2h interval. The 2 hours mark has been chosen because it is the boost time after which the reactor is expected to become subcritical. Really important to remember that these results do not come from the coupling and therefore doesn't show the real depletion of the fuel. They are instead time-stamp calculations obtained under the assumption of a constant neutron flux, hence a constant reaction rate, over the considered interval. These results will be compared in Chapter 6 with those from the coupled calculation, providing a clearer picture of how a time-dependent flux influences the observed depletion in the core. The concentrations of some isotopes in each ring are shown to illustrate the core's behavior, highlighting a higher depletion in the central ring due to its greater power density.

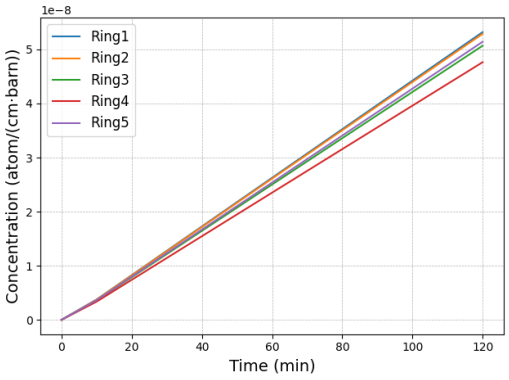

Figure 4.2: Ba-140 concentration over 2 hours

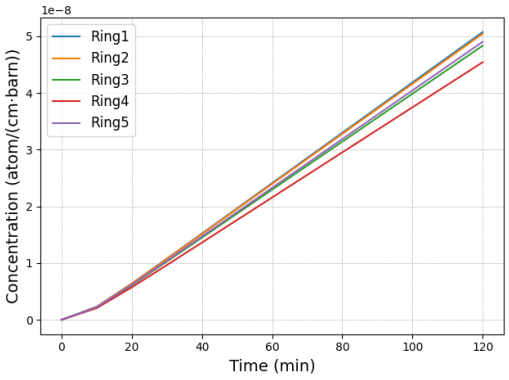

Figure 4.3: Cs-137 concentration over 2 hours

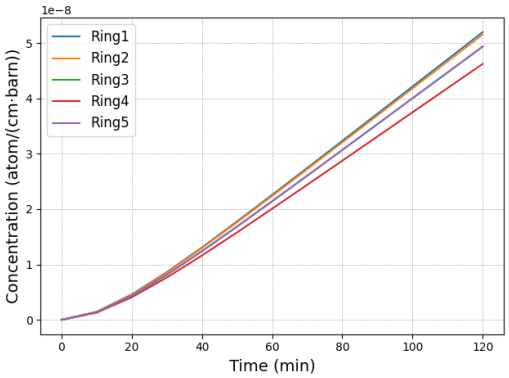

Figure 4.4: Zr-95 concentration over 2 hours

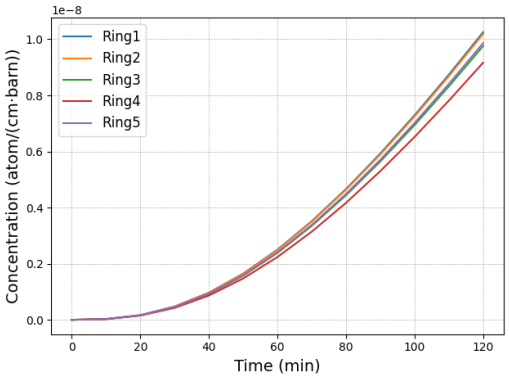

Figure 4.5: I-131 concentration over 2 hours

These behaviours were expected due to the Cumulative thermal Fission Yields (CFY) of U-235. CFY represent the amount of a given isotope produced per fission event, accounting for both direct formation and the decay of precursor isotopes. As shown in Table 4.2, the CFY of Iodine-131 is significantly lower than those of Cesium-137, Strontium-90, Barium-140 and Zirconium-95. This explains the slower increase in I-131 concentration observed in Figure 4.5, as compared to the more abundant isotopes with higher fission yields that ends up with a concentration about 5 times higher.

Isotopes	Cumulative Fission yield (%)
Iodine-131	2.878
Cesium-137	6.221
Strontium-90	5.73
Barium-140	6.314
Zirconium-95	6.502
Xenon-135	6.61
Krypton-85	0.286

Table 4.2: Cumulative Fission yield [26]

A particularly interesting case is illustrated in Figure 4.6, which shows an apparently unusual behavior in the production of Xenon-135 that despite having a much higher cumulative fission yield than I-131 (and in general higher than all the other displayed isotopes), presents a lower concentration at the 2 hour mark.

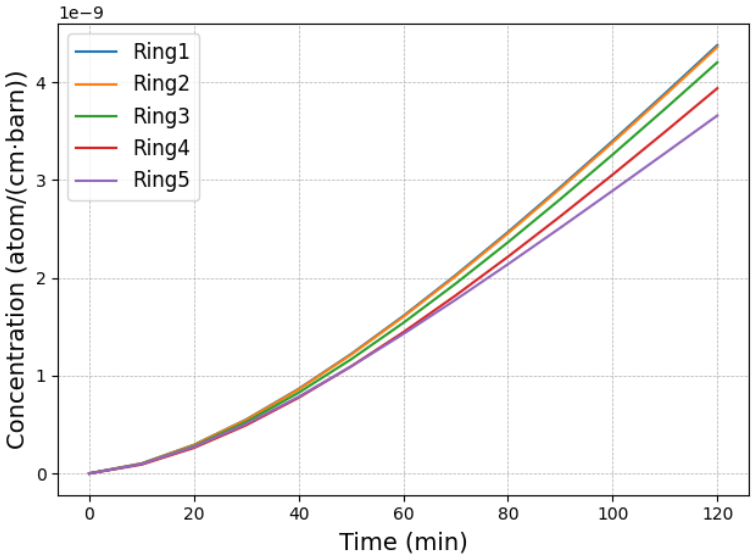

Figure 4.6: Xe-135 concentration over 2 hours

This seemingly counter-intuitive behaviour comes from the distinction between independent fission yields (IFY) and cumulative fission yields. While IFY represents the yield of nuclides produced directly from fission, CFY also includes contributions from beta decays of precursor fission products. In this context, the IFY values of Xe-135 and I-131 are not directly comparable, as the yield of I-131 is significantly

higher than that of Xe-135 [27]. This indicates that most Xe-135 is not produced directly by fission, but rather arises predominantly from the beta decay of precursors such as Iodine-135, which has a half-life of approximately 8 hours. Due of this delayed production, the initial build-up of Xe-135 is limited. Additionally, Xe-135 has an extraordinarily high capture cross section, making it extremely effective at absorbing neutrons. This property further contributes to its lower accumulation in the reactor core.
This strong absorption behavior is also why Xe-135 is often referred to as a "neutron poison" in reactor physics because it significantly reduces reactor reactivity by capturing neutrons more readily than most other fission products.

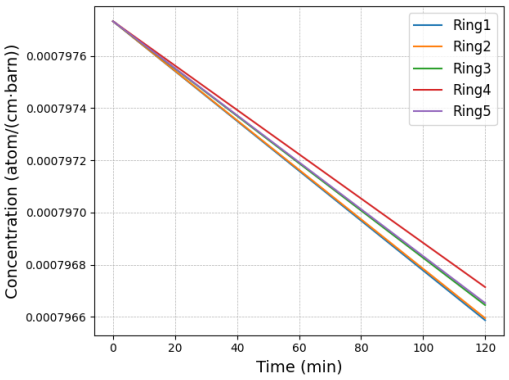

Figure 4.7: U-235 depletion in 2 hours

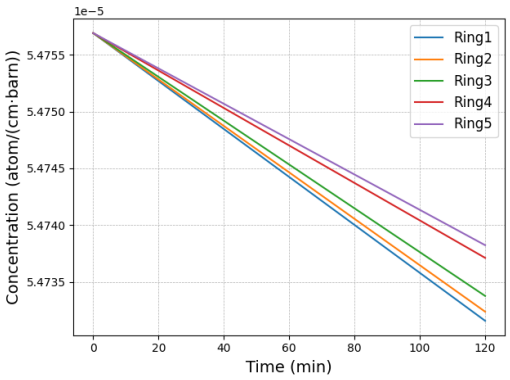

Figure 4.8: U-238 depletion in 2 hours

Same considerations can be done observing Figure 4.7 and 4.8. Due to their nature (fissile and fertile) both of their concentrations decrease in time due to fission and capture mechanisms.
It is possible to evaluate the percentage of Uranium burned after 2 hours, in the outermost core ring, using the following expression:

$$\%\text{Consumed} = \left(\frac{C_0 - C_{2\text{h}}}{C_0}\right) \times 100 \tag{4.6}$$

where C_0 and C_{2h} represent the initial concentration and the concentration after two hours, respectively.
The percentage of U-235 consumed (~0.1354 %) is substantially higher than that of U-238 (~0.0341 %), which can be attributed to the significant difference in their neutron interaction probabilities at thermal energies. Specifically, the microscopic fission cross section of U-235 is approximately 582.6 barns, whereas the neutron

capture cross section of U-238 is only about 2.683 barns [28]. This means that thermal neutrons are far more likely to induce fission in U-235 than to be captured by U-238, resulting in a much higher depletion rate of U-235 in a thermal reactor environment. This difference can be seen also from Figure 4.9, where the concentration of Plutonium is increasing (coming from U-238 capture) but is still a lot smaller than the fission products concentrations.

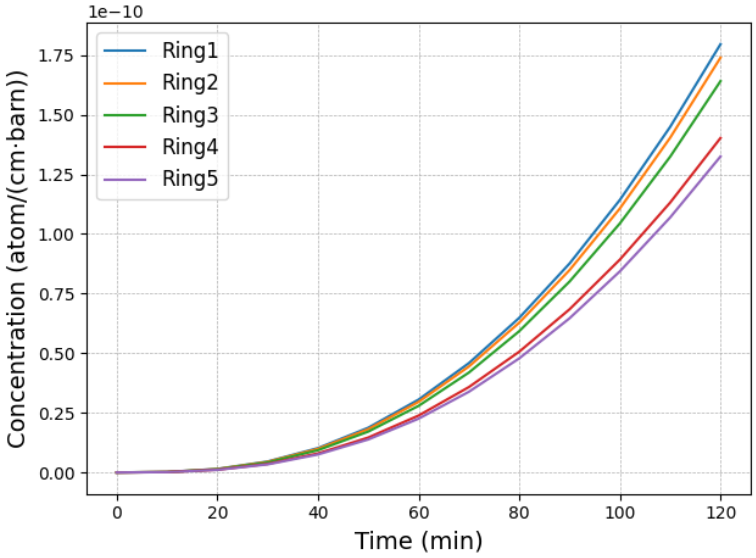

Figure 4.9: Pu-239 concentration over 2 hours

Decay heat computation

Beyond calculating the evolution of isotopic compositions in nuclear fuel, MENDEL can also be used to estimate the decay heat generated by spent fuel. This is particularly important in the context of my study, which focuses on a space-based NTP system. After shutdown, the reactor continues to produce heat due to the radioactive decay of fission products due to the 3 mechanisms cited in Subsection 4.1.1. In space, this residual heat represents a significant safety risk, especially given the limited options for heat rejection and system cooling. In the case of an NTP engine, the reactor is ideally shut down after about two hours of operation, primarily due to the rapid decrease in fissile isotopes and potential corrosion issues caused by prolonged exposure to high-temperature hydrogen. Accurate estimation of decay heat with MENDEL is therefore essential for evaluating post-shutdown thermal behavior and ensuring the safe handling and cool down of the reactor.

This is done and displayed in the following picture as a function of time after shutdown, for different reactor operation durations, i.e. "Boost duration":

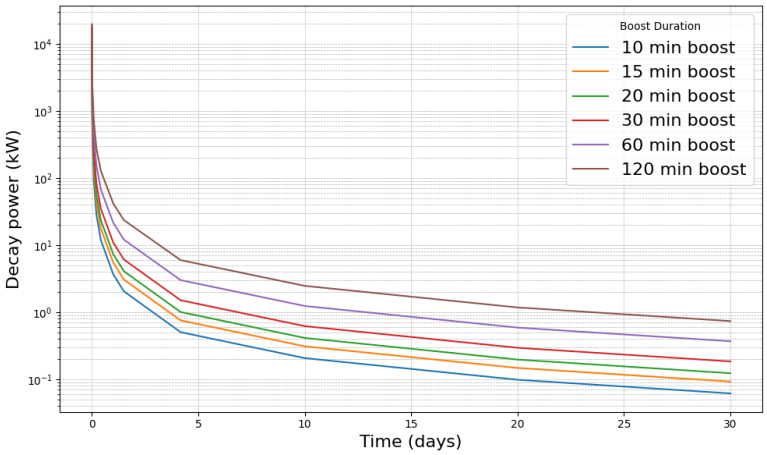

Figure 4.10: Decay heat evaluation in 30 days, with different Boost duration

Figure 4.10 illustrates the variation in decay heat for different boost durations. Longer boost durations result in higher residual heat, due to increased fuel depletion. It is important to note that these results were obtained using MENDEL in a non-coupled mode, meaning the data were produced independently from any feedback with TRIPOLI-5.

5 | The TRIPOLI-5-MENDEL Coupling structure

In this chapter, the methodology used to couple the stochastic neutronics code TRIPOLI-5 with the depletion code MENDEL is described. This coupling aims to enable detailed fuel depletion analysis within the SNRE reactor engine. The integration is facilitated by the C3PO coupling engine, which coordinates data exchange and controls the overall workflow. The following sections provide a detailed explanation of the coupling framework, including data flow mechanisms and implementation strategies.

5.1 ICoCo and C3PO

The ICoCo interface and the C3PO library have been adopted for the coupling.

ICoCo ICoCo stands for Interface for Code Coupling and it defines how a "Problem" should behave. The pure abstract C++ interface defines methods to a common mother class named "Problem" that each code has to provide in order for the supervisor to actually couple them. The supervisor performs the coupling algorithm, calling data exchanger objects and manipulating the data to exchange [29]. An overview of the coupling architecture can be see, in Figure 5.1.

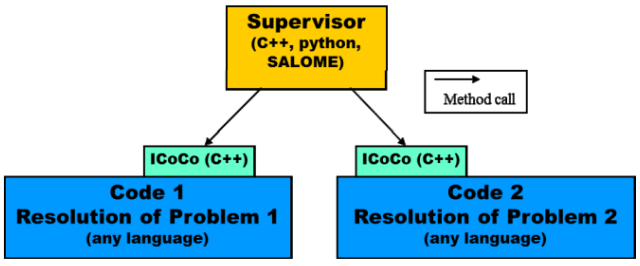

Figure 5.1: Overview of the ICoCo architecture [29]

This interface contains some method needed for the correct coupling. They can be divided in methods for initialization and termination of the code, methods for the time advancement of the code and methods for setting and getting informations. Some of them are mandatory and the most interesting are [29]:

Methods for initialization and termination of the code

- ***initialize()***, which initializes the code. It is called once before any other method. It returns *true* if everything is OK but if there's something wrong, *terminate()* will be called
- ***terminate()***, which terminates the computation, frees the memory and saves whatever needs to be saved. It is called once at the end of the computation

Methods for the time advancement of the code

- ***presentTime()***, which simply returns the current time t
- ***initTimeStep(dt)***, which takes as input the next dt (double) that will be used by the code. After its call, the computation step is defined to $]t, t + dt]$ where t is the value returned by *presentTime()*
- ***solveTimeStep()***, which actually computes the time step
- ***validateTimeStep()***, which advance the present time to the end of the computation time step

Methods that set and get informations Neither of the methods already defined in ICoCo have been used. Instead some functions that follow the same line of the latters have been created to allow the exchange of *numpy arrays*. They will be better explained in the 5.2, here below just a list of them:

- ***getArrayType()***
- ***setInputDoubleNpArray()*** and ***setOutputDoubleNpArray()***
- ***setInputStringNpArray()*** and ***setOutputStringNpArray()***

C3PO C3PO stands for Collaborative Code Coupling PlatfOrm. It is a Python-based coupling engine designed to standardize the implementation of multi-physics simulations. It builds upon ICoCo API, which encapsulates simulation codes as python classes. By following this standard, C3PO offers a flexible and general system to handle how simulations progress over time, share data between codes,

and check if the results are stable and accurate during the coupling process. A key advantage of C3PO is that it works independently of the specific codes it connects. It doesn't need to know how each code is built or what physical models it uses. Instead, it uses a common ICoCo interface, which makes it easy to connect different simulation tools, no matter what programming language they are written in or how they are structured. Even though in this work they haven't been used, C3PO's data exchanges are handled using MEDCoupling, a C++ library developed within the SALOME platform. Furthermore, C3PO is also made to work well in High Performance Computing (HPC) environments. It supports MPI (Message Passing Interface), which is the most commonly used method for running programs across multiple computers [30].
The structure of C3PO is based on three major pieces:

- **PhysicsDriver** is an abstract class that serves as a communication layer between C3PO and the coupled simulation codes via the ICoCo interface. It defines and standardizes the core functionalities that each code must implement to ensure compatibility within the coupling framework
- **Exchanger** is a class interface responsible for managing the exchange of information between different *PhysicsDriver* instances. This includes tasks such as data projection and interpolation on fields, which are handled using the MEDCoupling library
- **Coupler** is the component responsible for implementing the coupling logic and numerical algorithms. It is constructed using instances of *PhysicsDriver*, *Exchanger*, and *DataManager*. To perform a simulation, the user must create a custom class that inherits from *Coupler* and implements the *solveTimeStep()* method. If this method is not defined, a *NotImplementedError* will be raised during execution

5.2 Workflow of the coupling

The flow of thoughts used to structure the transient coupling is the following:

1. The simulation process begins with the execution of the TRIPOLI-5 code, which is encapsulated using the ICoCo API. During this step, the flux score is computed. This score is then processed directly within the TRIPOLI-5 code itself, as performing the manipulation internally was more straightforward and transparent. The resulting data is subsequently passed to C3PO
2. Subsequently, C3PO transfers the processed flux information to the MENDEL code using its *Exchanger* and *Coupler* modules

3. MENDEL requires the flux spectrum provided by TRIPOLI-5 in order to update the reaction rates. At this stage of the coupling process, the *Coupler* invokes the relevant methods of the MENDEL class, which is also encapsulated using the ICoCo API. This triggers the execution of the MENDEL simulation, where the updated nuclide concentrations are computed by solving the Bateman equations using the CRAM solver, as explained in Algorithm 3

4. The newly computed isotope concentrations are returned to C3PO, which then transfers them to TRIPOLI-5. The transient simulation continues iteratively until the final time step is reached

The coupling structure can be observed in the following picture:

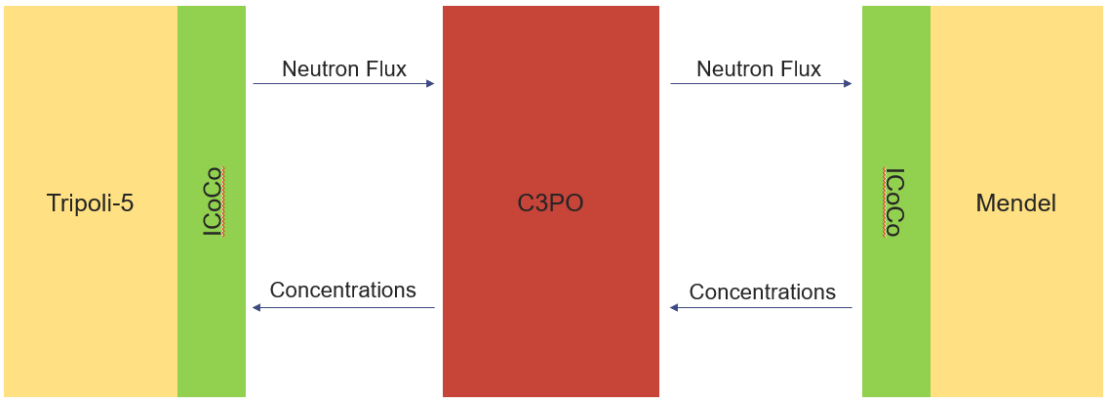

Figure 5.2: Structure of the coupling

To reach this coupling multiple objects have been created, in order:

PhysicsDriver To comply the C3PO need of physics drivers (to standardize each code via the ICoCo interface), two new drivers were created inheriting from the *ICoCoDriver* class: the *T5Driver* and the *MendelDriver*. They are equal in structure and are needed to exchange array types and to get and set input and output arrays (either double or string).

Algorithm 4 Class T5Driver/MendelDriver (inherits from ICOCODriver)

```
1: function getArrayType(name)
2:     return problem.getArrayType(name)
3: end function
4: function setInputDoubleNpArray(name, array)
5:     return problem.setInputDoubleNpArray(name, array)
6: end function
7: function getOutputDoubleNpArray(name)
8:     return problem.getOutputDoubleNpArray(name)
9: end function
10: function setInputStringNpArray(name, array)
11:     return problem.setInputStringNpArray(name, array)
12: end function
13: function getOutputStringNpArray(name)
14:     return problem.getOutputStringNpArray(name)
15: end function
```

where "problem" is the instance of each simulation code. This is the interface that, triggered by the coupler, triggers the exchange of informations.

Exchanger This stage required the most development effort, primarily due to the creation of a custom *ShortcutToArray* object and a new *ArrayExchanger* class, which inherits from the *LocalExchanger* class. These components were specifically designed to enable the exchange of `numpy` arrays directly, without relying on the MEDCoupling library. This approach is particularly promising, as it represents a significant step toward extending the applicability of C3PO to simulation codes that are not based on MEDCoupling.

Coupler For this work a *DepletionCoupler* has been built, inheriting from the common *Coupler* class. This coupler exploting two *PhysicsDriver* instances and the *Exchanger* instances make the coupling process possible, thanks to the creation of a *solvetimestep()* method that is constructed as it follows:

Algorithm 5 solveTimeStep method

```
1: function SOLVETIMESTEP
2:     list_driver ← ["T5", "MENDEL"]
3:     list_exch ← ["T5_2_MENDEL", "MENDEL_2_T5"]
4:     for all (item1, item2) in zip(list_driver, list_exch) do
5:         physicsDrivers[item1].solve()
6:         exchangers[item2].exchange()
7:     end for
8: end function
```

From the Algorithm 5 it can be observe how, with a for loop, each simulation code is ran and each information is exchanged between codes.
The whole C3PO coupling workflow can be seen in Figure 5.3:

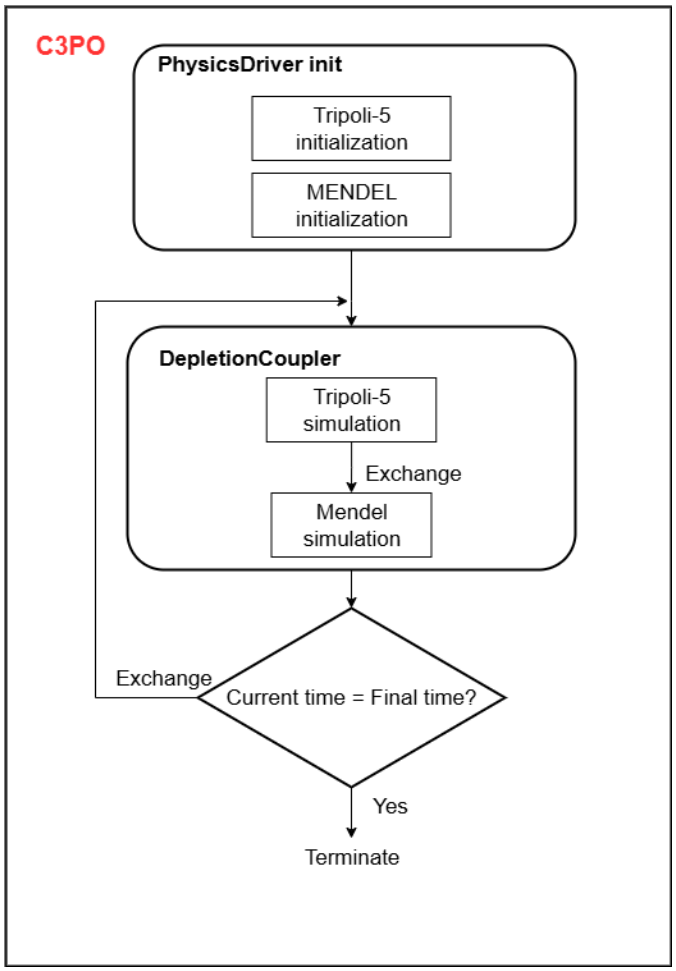

Figure 5.3: C3PO coupling workflow diagram

6 | Results and Considerations

This chapter presents the results obtained by from the coupling of the stochastic code TRIPOLI-5 with the depletion code MENDEL using the C3PO coupling engine. The simulations focus on the evolution of key physical parameters throughout the depletion process in the SNRE reactor engine. Outputs such as isotopic composition over time, neutron flux and related depletion quantities are shown to illustrate the proper behaviour of the transient coupled system. These result reflect the initial application of the developed coupling methodology and form the basis for further analysis and refinement.

6.1 SNRE results

The results obtained by the coupling are in accordance with what expected, starting from the accelerated rate of fuel depletion compared to the static approach. This behaviour arises from the transient nature of the coupling between the two codes, which ensures that the neutron flux and cross sections are continuously updated at each depletion step.
Because the coupling captures the changes over time, it gives a more realistic and dynamic picture of how the fuel behaves during depletion, which means the fuel composition evolves in response to actual changes in the reactor environment. This leads to faster changes in the isotopic makeup of the fuel, especially for fissile and fertile materials, since the system is constantly adapting based on the most current information from both the neutronics and depletion calculations.

6.1.1 Number of neutrons and k_{eff}

Since the fuel is undergoing fission, an increase of the number of neutrons in the reactor (and therefore of the neutron flux) is expected. This is showed in Figure 6.1, where it can be appreciated the number of source neutron changing over time:

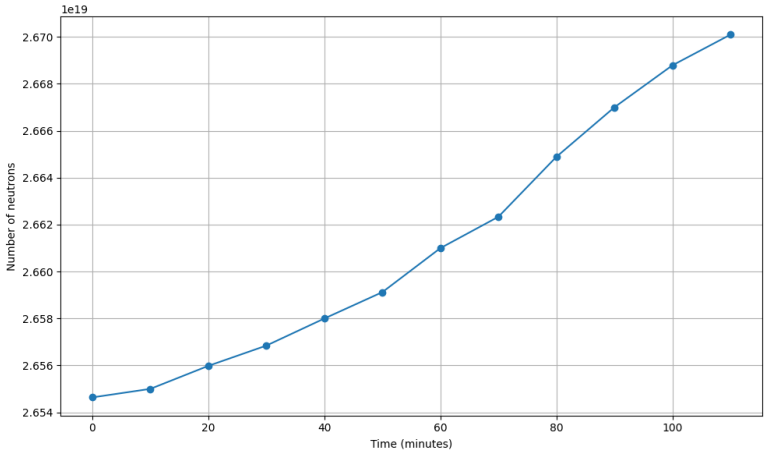

Figure 6.1: Number of source neutrons over time

The plot in Figure 6.2 shows the evolution of the effective multiplication factor, k_{eff}, over the first 7.5 hours of reactor operation. This trend provides insight into the reactivity behavior of the system under sustained power conditions.

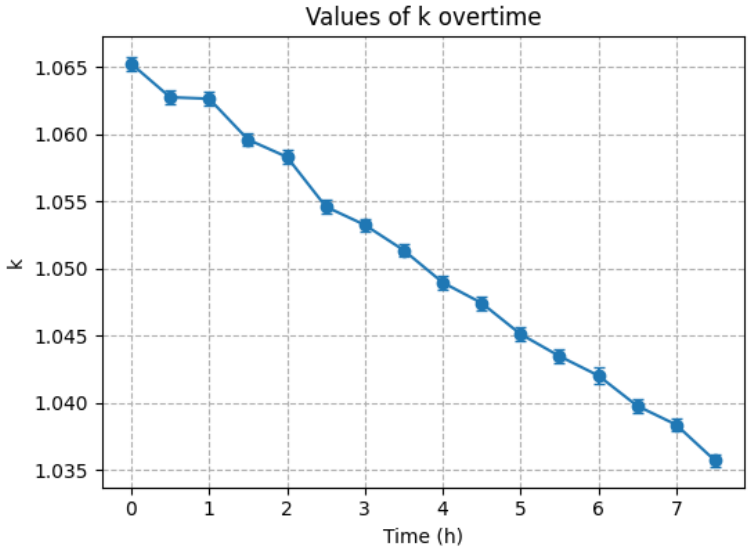

Figure 6.2: k_{eff} over 7.5 hours time

As shown in Figure 6.2, k_{eff} decreases significantly over the course of just under 8 hours. However, this reduction is not as sharp as initially expected for this NTP system. A steeper drop in reactivity was anticipated, particularly during the

first two hours of operation, when k_{eff} was expected to fall from its initial value of approximately 1.06 to below 1.0. Such a drop would have made the reactor subcritical and effectively unusable for continued propulsion.
The less pronounced drop observed in the simulation can be attributed to two main limitations in the current modeling approach.

Axial division First, the reactor core was segmented only radially into concentric rings, without any axial division. As a result, axial variations in fuel depletion, especially in regions exposed to higher power densities along the height of the core, are not captured. Introducing axial segmentation would have provided a more detailed and realistic depletion profile, but was not feasible within the scope of this work due to the significant increase in model complexity and computational workload. This challenge is further complicated by the current structure of the T5 code, which does not easily support coupling across a large number of spatial regions, making such refinement exponentially more time-consuming. However, this limitation is specific to the current version of the code and will be addressed in future developments.

Corrosion mechanism The second factor is the absence of corrosion modeling. In reality, corrosion of the fuel elements, particularly under high-temperature hydrogen flow, can lead to material loss and structural degradation. These effects would likely accelerate the decrease in reactivity. Since this mechanism is not accounted for, the simulation tends to underestimate the actual depletion behavior of the system. The Hydrogen corrosion process is influenced by multiple NTP design factors [31]:

- **Propellant temperature and pressure:** Higher temperatures and pressures increase the chemical reactivity of hydrogen, thereby accelerating corrosion rates
- **Operation time and duty cycle:**. Longer operating times and more frequent cycling result in greater cumulative depletion and thermal stress, both of which can exacerbate corrosion effects
- **Propellant mass flow rate:** This factor presents a more complex relationship. Higher flow rates reduce the contact time between the reactor materials and the hydrogen propellant, which can mitigate corrosion and erosion. However, beyond a certain threshold, excessive flow can introduce mechanical erosion and thermal stress, potentially worsening material degradation
- **Fuel matrix composition and form**

To mitigate the adverse effects of hydrogen-induced corrosion observed during early NTP development, a thin protective coating have been applied to the surface of each individual fuel elements. This approach has proven effective in significantly reducing, though not fully eliminating, material degradation. Specifically, the introduction of a thin protective coating layer has led to a substantial decrease in fuel mass loss during reactor operation. Empirical data indicate that early NTP fuel elements can experience fuel depletion rates as high as approximately 1 gram/minute per Fuel Element during boost-phase operation [31]. With the application of the protective coating, this rate is reduced to approximately 0.2 gram/minute per Fuel Element, representing an 80% reduction in fuel loss.
Although the application of protective coatings significantly reduced the rate of fuel loss, the remaining erosion is still substantial. For an operational period of two hours, with 564 fuel elements and a loss rate of 0.2 grams per minute per element, the total fuel loss adds up to:

$$\text{Total loss} = 0.2\,\frac{\text{g}}{\text{min}} \times 120\,\text{min} \times 564 \approx 13.5\,\text{kg}$$

This means that more than 13 kilograms of fuel can be lost during a single engine burn. Given a total fuel mass of approximately 373 kilograms, this corresponds to a loss of about 3.6% of the total fuel inventory. Despite the improvements brought by the coating, this level of material degradation is still quite considerable compared to the actual fuel consumption through fission. After 2 hours of operation, the total U-235 consumption is only ~0.1354 %, which is significantly lower than the expected fuel loss due to corrosion. In this study, this effect is not modeled, which introduces a degree of approximation. As a result, the simulated drop in k_{eff} is likely smaller than what would be observed in a more detailed model that accounts for continuous fuel loss over time.

6.1.2 Isotopes concentration

As expected, due to the gradual increase in neutron flux over time, the coupled simulation results in a higher degree of fuel depletion compared to the uncoupled case. This is because, in the coupled approach, the evolving material composition at each time step directly affects the neutron transport calculations in the subsequent step, creating a more realistic feedback between burnup and flux distribution.
This effect can be observed in the Figures 7.4 and 7.6, where the concentrations of U-235 and U-238 show a more pronounced reduction in the coupled scenario.

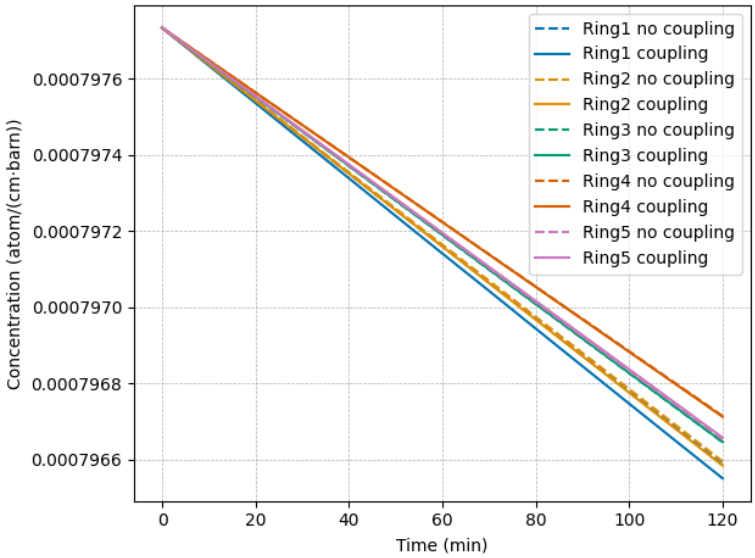

Figure 6.3: U-235 concentration comparison

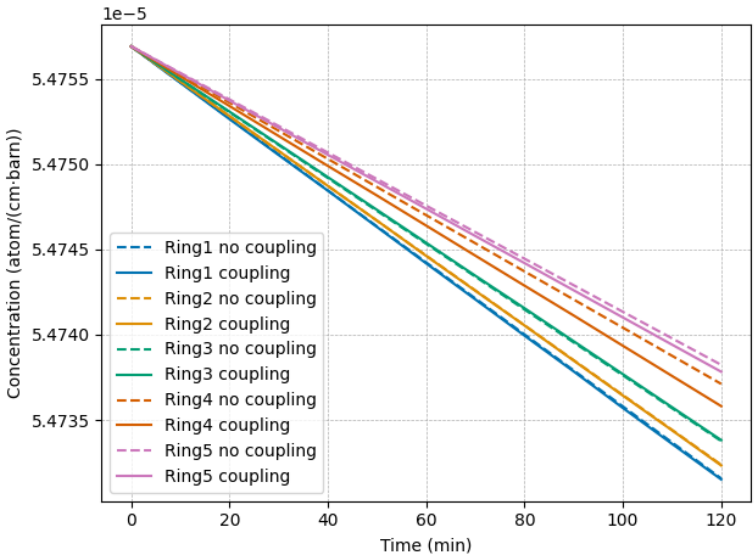

Figure 6.4: U-238 concentration comparison

A similar trend can be seen in Figures 7.8 and 7.7, where the buildup of Pu-239 and Xe-135 is more significant in the coupled case. The uncoupled case, by contrast,

underestimates the depletion, as it neglects the dynamic interplay between neutron flux evolution and isotopic changes over time.

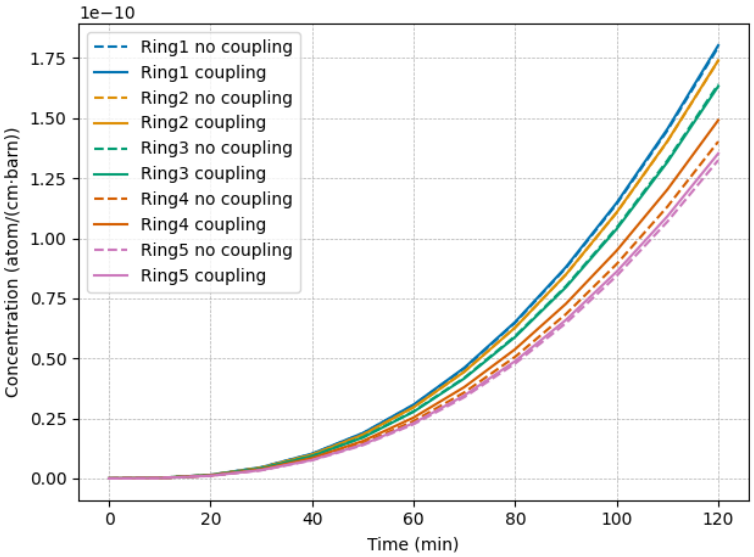

Figure 6.5: Pu-239 concentration comparison

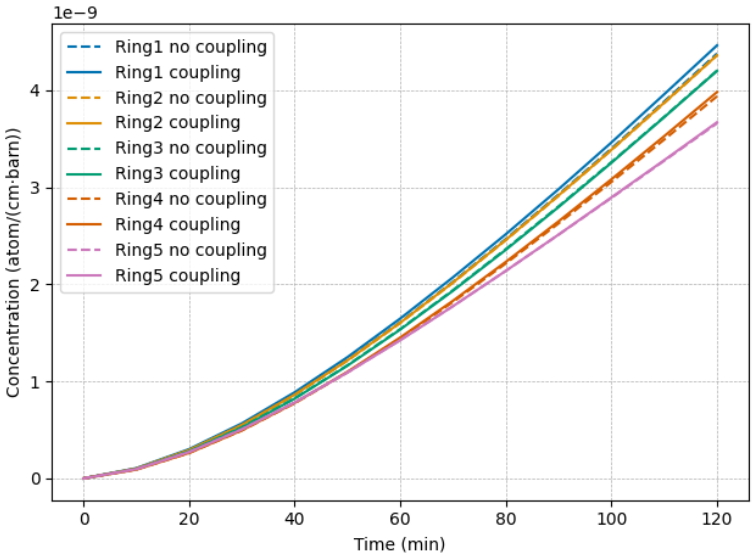

Figure 6.6: Xe-135 concentration comparison

6.1.3 Decay heat

In this analysis, the decay heat is evaluated following a 2-hour boost phase of the NTP system, during which the reactor operates continuously.

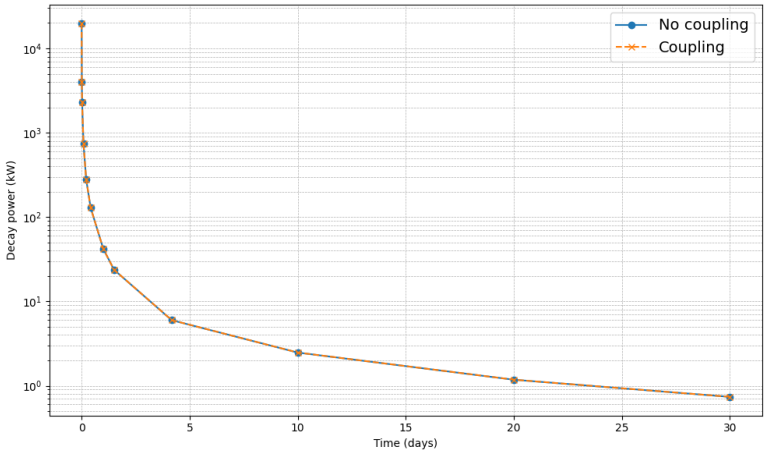

Figure 6.7: 2 hours boost decay heat comparison

Even though from Figure 6.7 we can't really observe differences, they are still present. What is expected is a small increase in decay heat in the case of the coupling due to the increased burnup.

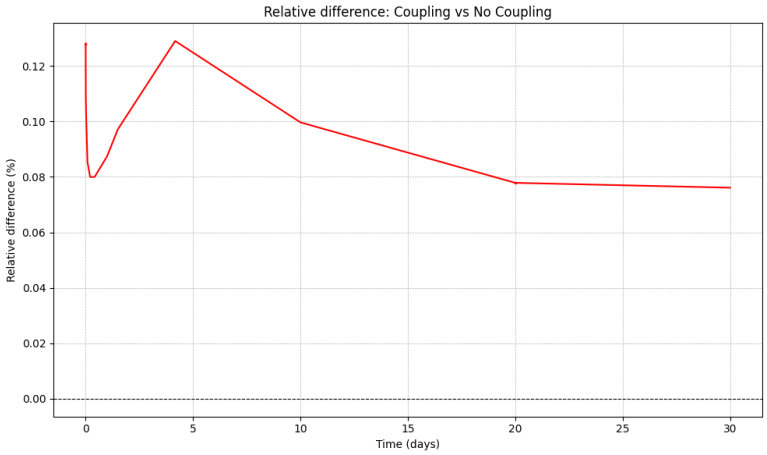

Figure 6.8: 2 hours boost relative difference decay heat

The trend observed in the in Figure 6.8 is, once again, consistent with expectations. Since the coupled simulation results in a higher degree of fuel depletion, the corresponding decay heat is also greater. This is primarily due to the increased buildup of fission products and activation products, that accumulate as a result of more intense neutron irradiation over time. The coupled case, by better capturing the progressive changes in isotope concentrations and neutron flux, yields a more realistic estimate of the post-operation decay heat, which is a critical parameter for thermal management and reactor safety during shutdown. The difference can also be observed in Table 6.1:

Time (days)	**No-coupling Heat (kW)**	**Coupling Heat (kW)**
0.000012	19778.44	19803.77
0.006944	3976.57	3980.91
0.020833	2303.60	2305.96
0.083333	749.67	750.31
0.208333	280.67	280.89
0.416667	128.81	128.92
1.000000	41.99	42.03
1.500000	23.70	23.72
4.166667	5.99	6.00
10.000000	2.47	2.48
20.000000	1.18	1.18
30.000000	0.74	0.74

Table 6.1: Comparison of decay heat with and without coupling

7 | Verification Study

Since the main coupling work was finished ahead of schedule, there was time to carry out a verification study to check that the new coupling between TRIPOLI-5 and MENDEL works properly. Although both codes have already been validated separately, the way they were linked together in this project hadn't been tested yet. To do this, a simple fuel pin model was used, and the results from the new T5-MENDEL coupling were compared to those from the already validated TRIPOLI-4 (T4) depletion calculations. Because T4 and MENDEL have been thoroughly tested before, their results act as a solid reference to see if the new coupling gives consistent and reliable results. The setup was kept simple to focus on checking the coupling itself without other complications.

7.1 Problem definition

7.1.1 Geometry definition

The geometry chosen for the verification study is a simple fuel pin surrounded by a layer of cladding and by a moderator. The minimal setup was chosen to reduce the complexity of the simulation and isolate as much as possible the behaviour of the coupling itself.By avoiding more detailed features like assemblies or control rods, it's easier to focus on checking whether the T5-MENDEL coupling gives results consistent with what's expected.

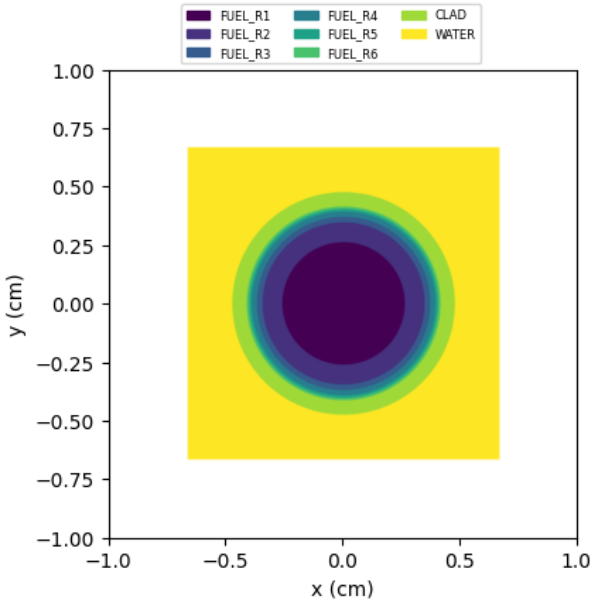

Figure 7.1: Radial section of the fuel pin

Figure 7.2: Axial section of the fuel pin

As can be seen from Figure 7.1, the pin has been radially divided in six regions to capture the variation in fuel depletion as a function of distance from the center. Surrounding the pin there's water, which is able to moderate the neutron and increase the fission probability. To simulate a critical core based on this pin model, reflective boundary conditions were applied to all boundaries of the geometry.

7.1.2 Simulation definition

Also in the simulation definition, things have been kept simple: the particle chosen is the Neutron, the source is a mono-kinetic point isotropic source of 2 MeV. To make the verification process possible the nuclear data file, chain data file and GENDF files were shared between the T4 and T5 codes. On top of this also the same energy mesh, to get the flux score, was used. Due to the large computation time it wasn't possible to simulate with more than 5000 particles, in Table 7.1 the simulation parameters of both codes:

Code	Nb of neutrons	Nb of batches	Discarded batches
T5 - T4	5000	150	50

Table 7.1: Simulation parameters

7.2 Steady-state results comparison

To get the a meaningful comparison, it's essential to have the same exact configuration, more specifically the steady-state configuration, before considering any depletion effects. To statistically compare the results of the two Monte Carlo simulations the reported values of k_{eff} and their associated statistical uncertainties σ were analyzed. The standardized distance between the two sample means is evaluated with the *z-score*, which is computed as:

$$z = \frac{k_1 - k_2}{\sqrt{\sigma_1^2 + \sigma_2^2}} \tag{7.1}$$

And then the two-tailed test (testing the discrepancy of the analyzed value in either direction):

$$p = 2 \cdot (1 - \Phi(|z|)) \tag{7.2}$$

where Φ is the the Cumulative Distribution Function of the standard normal distribution. The threshold level of $\alpha = 0.05$ was chosen as a convention. If $p < \alpha$ it indicates that the two results are not statistically compatible, meaning that there is a statistical difference between the means [32]. The steady-state results of the two codes are:

Simulation	k_{eff}	σ
T4	1.196677	8.17e-04
T5	1.196642	0.00102

Table 7.2: Simulation results

with an evaluated p value of:

$$p = 0.979$$

and a difference in *pcm* of just 3.5, indicating the statistical compatibility of the steady-state results and therefore confirming the identical starting configuration.

Also the flux score per unit lethargy of the steady-state can be compared:

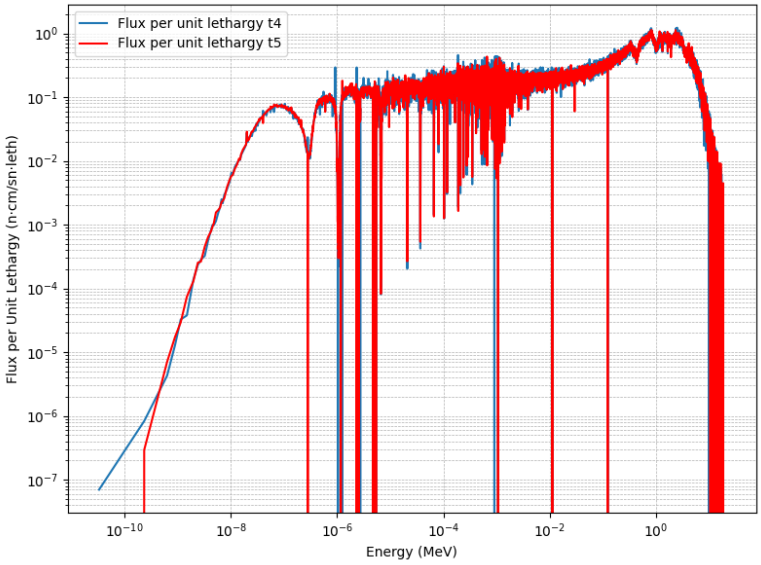

Figure 7.3: Flux comparison

where the small differences that can be seen from Figure 7.3 are due to statistical uncertainty given by the stochastic nature of particle sampling.
Having established that the steady-state solutions are statistically compatible, we can now proceed to compare the results concerning the depletion and therefore of the actual T5-MENDEL coupling

7.3 Depletion results comparison

The comparison between the results obtained from T4 and the T5-MENDEL coupling shows a good agreement during the steady-state phase. The values are statistically compatible within the expected uncertainties. However as depletion progresses over a large number of time steps, discrepancies begin to appear in the concentrations of the isotopes. The discrepancy can be attributed to two primary factors:

1. The relatively low amount of particles (5000 particles per cycle) and cycles (150) used in the two simulations contributes to increased statistically uncertainty. This choice was made to maintain manageable computational costs, but it results in less precise neutron flux estimates. Such uncertainties can propagate through the depletion calculations, leading to growing deviations over time.

2. There is a fundamental structural difference in the depletion methodologies employed by the two systems. In the T4 + MENDEL approach, reaction rates are directly computed by T4 and subsequently passed to MENDEL for depletion calculations. Conversely, in the T5-MENDEL coupling developed in this work, TRIPOLI-5 provides only the neutron flux, while reaction rates are calculated within MENDEL based on cross-section data. This additional processing step introduces another source of uncertainty, particularly if discrepancies exist in cross-section handling or energy group structures compared to those used internally by TRIPOLI-4.

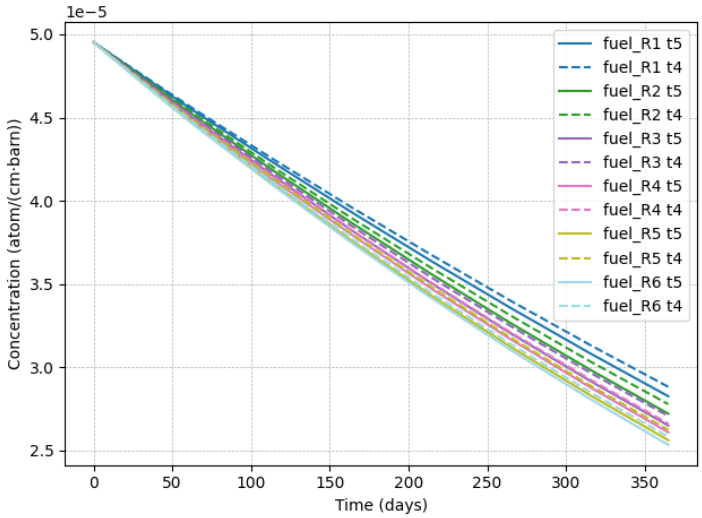

Figure 7.4: U-235 concentration comparison

As a result of those combined effects, the T5-MENDEL coupling tends to show a slightly more advanced depletion overtime, with a lower concentration of fissile and fissionable nuclides, Figure 7.4 and 7.6, and a higher accumulation of fission products and PU239 compared to T4, Figure 7.7, 7.9 and 7.8.

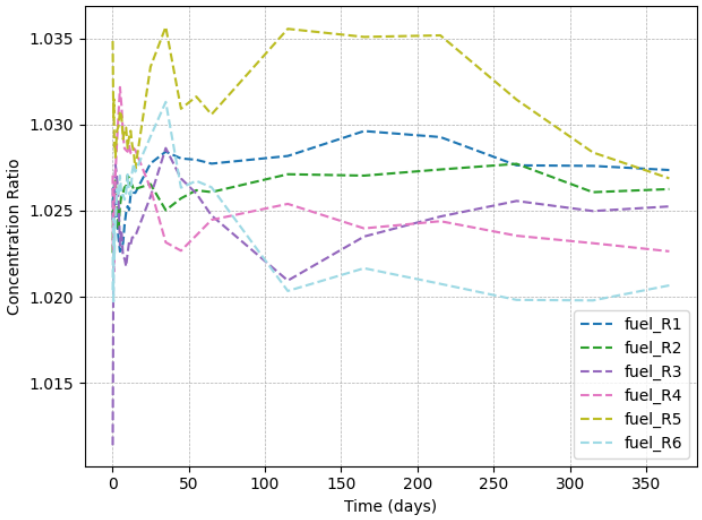

Figure 7.5: Ratio of change in U-235 concentration

Figure 7.5 shows the discrepancy between the results obtained from the two codes, with differences in the U-235 concentration ranging from 2.1% to 2.7% after one year of irradiation.

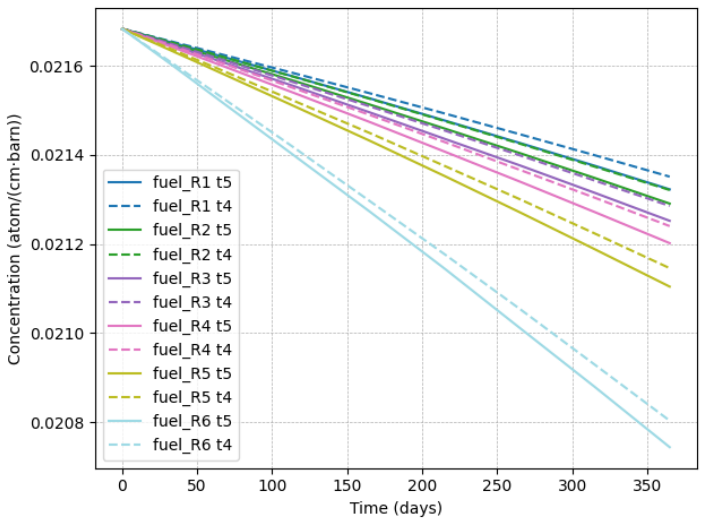

Figure 7.6: U-238 concentration comparison

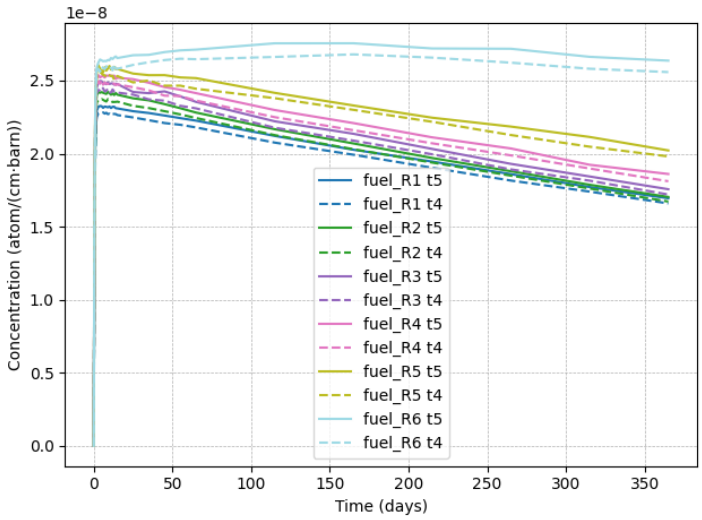

Figure 7.7: Xe-135 concentration comparison

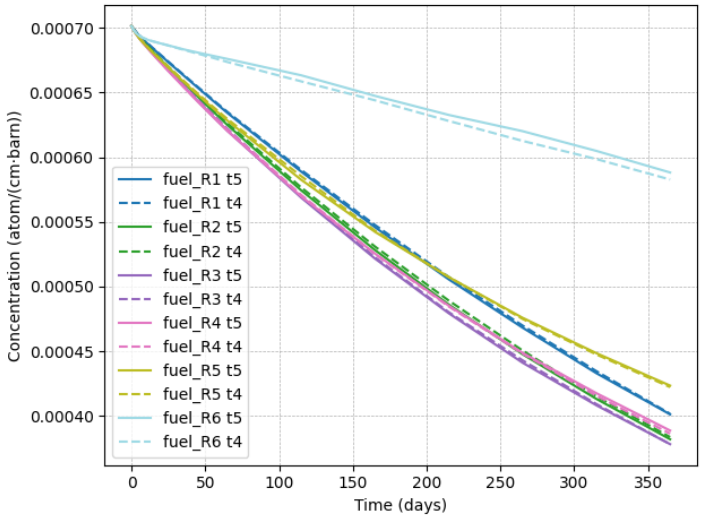

Figure 7.8: Pu-239 concentration comparison

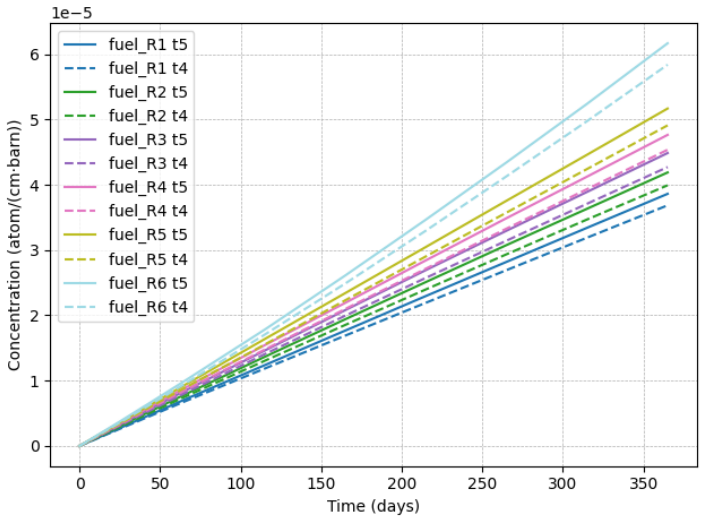

Figure 7.9: Cs-137 concentration comparison

More broadly, the discrepancies for most other isotopes remain below 5%, indicating a generally good level of agreement between the two results. These relatively small differences are likely due to statistical uncertainties associated with the relatively low number of particles used in the simulation. Nonetheless, the overall depletion behavior is consistently reproduced, confirming the reliability of the coupling for isotopic evolution analysis over the simulated irradiation period.

8 | Conclusions and Perspectives

8.1 Conclusions

The main objective of the thesis was to develop and apply a transient coupling between the transport Monte Carlo code TRIPOLI-5 and the depletion code MENDEL, in order to obtain a more realistic isotopic evolution of the fuel compared to the uncoupled approach. The coupling architecture was implemented through the extensive use of ICoCo and C3PO CEA tools, defining a workflow in which the two codes are executed in sequence and exchange the necessary quantities at each time step.

From the software point of view, one of the most relevant results of the work is the realization of a modular and reusable workflow, where dedicated components (such as drivers, exchangers and couplers) were implemented to make the data exchange more robust and as independent as possible of the specific assumptions of the case study. In particular, the introduction of a data-exchange mechanism based on numerical arrays (NumPy) without relying on the MEDCoupling library represents an interesting step towards the extension of the C3PO framework to codes that are not natively based on that library.

The application to the SNRE study revealed a behaviour consistent with physical expectations. The coupling allows to dynamically update the neutron flux and the isotopic concentrations, producing a faster depletion compared to the uncoupled case and therefore a more realistic isotopic evolution. In particular, the variation of the U-235 and U-238 concentrations as well as the isotopic inventory build-up of Pu-239 and Xe-135 follow expected physical trends, highlighting the capability of the coupled approach to capture the feedback between composition and neutron transport.
Regarding the integral quantities, the k_{eff} trend highlights a significant reduction, but less marked than initially expected for this NTP concept. This observed behaviour was mainly due to the absence of a corrosion/erosion modelling for fuel operating in high-temperature hydrogen. As discussed in paragraph 6.1.1, after

a 2-hour boost the estimated fuel loss due to corrosion can reach about 13 kg, corresponding to roughly 3.6% of the total fuel inventory, while the depletion-driven consumption of U-235 over the same period is only 0.1354%. This large difference indicates that, for the SNRE operating conditions considered, fuel loss mechanisms may dominate the reactivity evolution and can therefore mask or outweigh the effect of isotopic depletion if they are not accounted for. Nevertheless, developing and implementing a dedicated corrosion model was outside the scope of the internship and of the present work, so the analysis was focused on the TRIPOLI-5–MENDEL coupling and on depletion-related effects. A second contributing limitation is the lack of axial segmentation, since the core is discretized only radially and not along the axial direction.

In parallel, a **decay heat evaluation** was discussed after a 2-hour boost. The comparison between the coupled and uncoupled case showed a higher depletion and therefore higher accumulation of fission products in the coupled case, resulting in a slightly higher residual power after shutdown. Again, this follows the expected physical behaviour.

Finally, it was possible to perform a **verification study** of the coupling, comparing the TRIPOLI-5–MENDEL framework with a reference solution based on TRIPOLI-4 in a simplified problem (fuel pin). Steady state results are statistically compatible, providing a solid basis for neutron transport comparison. During depletion, differences in the isotopic concentrations slowly grow with time steps but generally remain in a reasonable range (usually a few percentage points, with most species below 5%). These discrepancies are mainly attributed to the limited number of particles used to keep the computational time manageable, and to a structural difference in how reaction rates are obtained (directly within TRIPOLI-4 in the reference workflow, or reconstructed in MENDEL from the flux provided by TRIPOLI-5).
Overall, the results indicate that the coupling operates correctly, remains stable throughout the simulation, and provides a reliable basis both for isotopic evolution analyses and for future extensions towards more advanced models and applications.

8.2 Perspectives and future developments

Even though the coupling framework showed coherent results, future development paths can be followed to increase its physical accuracy and numerical robustness:

1. **Axial segmentation** of the core. Introducing a discretization along the axial direction of the reactor's core could allow the capture of axial variations in the power, flux and burnup, obtaining a more realistic depletion of the fuel.

2. **Corrosion/erosion modeling of the fuel**. As previously discussed, in a NTP system, high-temperature hydrogen corrosion has a significant and critical role in the fuel mass loss and therefore on the lifetime and reactivity of the reactor.

3. **Increase the number of particles**. In order to reduce the uncertainty on the neutron flux and therefore on the depletion process, a higher number of particles and batches can be adopted.

4. **Extension of the framework to other feedback codes**. The framework can be extended to other physics (by including thermal models or simplified feedbacks) while keeping the same modular and reusable nature.

5. **Progressive verification on more representative benchmarks**. The verification process can be extended to more complex cases (with more regions, more materials and different geometries).

In summary, this work shows that the TRIPOLI-5–MENDEL coupling is fully operational and delivers consistent results. At the same time, it clearly highlights which physical factors (such as axial segmentation and corrosion effects) and which numerical aspects (such as Monte Carlo statistics and reaction-rate processing) are the main drivers for improving fidelity and predictive capability in future applications.

Annex

In these tables, the concentrations of isotopes are given in $atom/(cm \cdot barn) \cdot 10^{24}$:

Tungsten

Isotopes	Concentrations
W182	0.016773407575112604
W183	0.009057576600560361
W184	0.01939377129515554
W186	0.017994977402590834

Table 8.1: Tungsten data

Lithium

Isotopes	Concentrations
LI6	0.06695325749485338
H1	0.0665841950635175

Table 8.2: Lithium data

H2 above the reactor

Isotopes	Concentrations
H1	0.0031550033737115088

Table 8.3: H2 above the reactor data

Aluminum

Isotopes	Concentrations
CU63	0.0007989408967112522
CU65	0.0003561007377835631
MG24	0.0008132003255001749
MG25	0.00010295008579489054
MG26	0.00011334784590575648
MN55	0.00018218336667473296
AL27	0.057806361631080036

Table 8.4: Aluminum data

H2 below the reactor

Isotopes	Concentrations
H1	0.000378241881734732

Table 8.5: H2 below the reactor data

Vessel

Isotopes	Concentrations
CU63	0.0007989408967112522
CU65	0.0003561007377835631
MG24	0.0008132003255001749
MG25	0.00010295008579489054
MG26	0.00011334784590575648
MN55	0.00018218336667473296
AL27	0.057806361631080036

Table 8.6: Vessel data

Reflector, Drums, Barrel

Isotopes	Concentrations
BE9	0.12348724194277

Table 8.7: Reflector, Drums, Barrel data

Control plates

Isotopes	Concentrations
B10	0.004095414446082208
B11	0.016484557644783158
CU63	0.020579972090865366

Table 8.8: Control plates data

Graphite

Isotopes	Concentrations
C12	0.08533698998271992
B11	9.299104014560937e-08

Table 8.9: Graphite data

H2 supply

Isotopes	Concentrations
H1	0.0031550033737115088

Table 8.10: H2 supply data

Tie bolt

Isotopes	Concentrations
MO92	0.0001859974366001452
MO94	0.00011346800408156624
MO95	0.0001931878384838293
MO96	0.00020034435923085609
MO97	0.0001135203337172889
MO98	0.00028390412006412707
MO100	0.00011103249322498426
SI28	0.0007911255030636895
SI29	3.875904999137334e-05
SI30	2.47400625018711e-05
CR50	0.0007507071772678587
CR52	0.013940372396938497
CR53	0.0015486664850647535
CR54	0.00037799691192010347
MN55	0.001572566009869757
FE54	0.00330300903921921
FE56	0.05036982392995527
FE57	0.001186943128401209
FE58	0.00014846343391545347
CU63	0.0005275606679547377
CU65	0.00022790438115337147
NI58	0.006874611954788672
NI60	0.002540707783151523
NI61	0.00010819360901261962
NI62	0.0003381987458222932
NI64	8.304502713125069e-05
N14	0.00023904689408344484
N15	8.242678170384963e-07
C12	0.0001200241831427795
P31	4.648709215305846e-05
S32	2.1380931210724503e-05
S34	9.092600909302344e-07
S33	1.6595174279631097e-07

Table 8.11: Tie bolt data

Inner tie tube, Outer tie tube and Coat

Isotopes	Concentrations
ZR90	0.020201610596584946
ZR91	0.004405482427476834
ZR92	0.00673387019886165
ZR94	0.006824178662169998
ZR96	0.0010994073794059836
C12	0.03926454926449941

Table 8.12: Inner tie tube, Outer tie tube and Coat data

Moderator

Isotopes	Concentrations
ZR90	0.018645459267699536
ZR91	0.004066118124655537
ZR92	0.006215146498264704
ZR94	0.006298514941106025
ZR96	0.00101471718172559
H1	0.07191722989839222

Table 8.13: Moderator data

H2 return

Isotopes	Concentrations
H1	0.000378241881734732

Table 8.14: H2 return data

Fuel H2

Isotopes	Concentrations
H1	0.0006333908288132953

Table 8.15: H2 passing in the fuel holes data

Fuel

Isotopes	Concentrations
U235	0.0007977332385712781
U238	5.475690608828454e-05
ZR90	0.006773595790972409
ZR91	0.0014771583040542025
ZR92	0.0022578647428646644
ZR94	0.0022881475406048373
ZR96	0.0003686304978865397
C12	0.06890717840675467

Table 8.16: Fuel data

Bibliography

[1] NASA Glenn Research Center. *Nuclear Thermal Propulsion Systems*. Accessed: 2025-06-06. 2024. URL: https://www1.grc.nasa.gov/research-and-engineering/nuclear-thermal-propulsion-systems/ (cit. on pp. 1, 2, 9, 10).

[2] G. P. Sutton and O. Biblarz. *Rocket propulsion elements. John Wiley & Sons, 2011.* Accessed: 2025-08-22 (cit. on p. 5).

[3] C. Singaram. *Rocket Science 101 Explained!* Accessed: 2025-08-22. URL: https://www.chendurs.com/all-newsletters/rocket-science-101-explained (cit. on p. 6).

[4] L3Harris Technologies. *RS-25 Engine*. Accessed: 2025-06-06. 2024. URL: https://www.l3harris.com/all-capabilities/rs-25-engine (cit. on p. 7).

[5] Wikipedia contributors. *SpaceX Starship — Wikipedia, The Free Encyclopedia*. Accessed: 2025-06-06. 2025. URL: https://en.wikipedia.org/wiki/SpaceX_Starship (cit. on p. 7).

[6] S. K. Borowski, D. R. McCurdy, and T. W. Packard. «Nuclear thermal rocket/vehicle characteristics and sensitivity trades for nasa's mars design reference architecture (dra) 5.0 study». In: 2009. URL: https://api.semanticscholar.org/CorpusID:4247857 (cit. on p. 8).

[7] NASA Glenn Research Center. *Typical Components of Nuclear Thermal Propulsion Systems*. Accessed: 2025-06-06. 2024. URL: https://www1.grc.nasa.gov/research-and-engineering/nuclear-thermal-propulsion-systems/typical-components/ (cit. on p. 8).

[8] Culbreth W. Lawdensky V. J. *Computational Analysis of Nuclear Thermal Propulsion Rocket Fuel and Prospective Coating Materials*. Tech. rep. Accessed: 2025-06-06. University of Nevada, Las Vegas, 2018. URL: https://arc.aiaa.org/doi/10.2514/6.2018-4674 (cit. on pp. 11, 12, 33, 35).

[9] F. P. Durham. *Nuclear Engine Definition Study Preliminary Report, Volume 1 - Engine Description*. Tech. rep. Accessed: 2025-06-01. . Los Alamos, NM (USA):Los Alamos National Laboratory, 1972 (cit. on pp. 13, 14).

[10] Y. A. Kazansky. «0 - Introduction to nuclear power technology». In: (2020), p. 10. DOI: https://doi.org/10.1016/B978-0-12-818483-7.10000-9. URL: https://www.sciencedirect.com/science/article/pii/B9780128184837100009 (cit. on p. 17).

[11] CEA CNRS and contributors. «Neutron Moderators». In: (). URL: https://radioactivity.eu.com/articles/phenomenon/neutrons_moderators (cit. on p. 18).

[12] Nuclear Power. *Neutron Capture - Cross Section*. Accessed: 2025-06-04. URL: https://www.nuclear-power.com/nuclear-power/reactor-physics/nuclear-engineering-fundamentals/neutron-nuclear-reactions/neutron-capture-radiative-capture/neutron-capture-cross-section (cit. on p. 19).

[13] A. Coronetti, R. Alia, D. Lucsanyi, M. Letiche, M. Kastriotou, C. Cazzaniga, C. Frost, and F. Saigne. «An Analysis of the Significance of the 14 N(n, p) 14 C Reaction for Single-Event Upsets Induced by Thermal Neutrons in SRAMs». In: *IEEE Transactions on Nuclear Science* PP (Aug. 2023), pp. 1–1. DOI: 10.1109/TNS.2023.3239407 (cit. on p. 20).

[14] «Evaluated Nuclear Data File (ENDF) Retrieval & Plotting». In: (). URL: https://www.nndc.bnl.gov/sigma/ (cit. on pp. 21, 22).

[15] Energy Encyclopedia. «Absorber». In: (). Accessed: 2025-06-03. URL: https://www.energyencyclopedia.com/en/nuclear-energy/the-nuclear-power-industry/absorber (cit. on p. 22).

[16] Nuclear Power. *Six-Factor Formula – Effective Multiplication Factor*. Accessed: 2025-06-05. URL: https://www.nuclear-power.com/nuclear-power/reactor-physics/nuclear-fission-chain-reaction/six-factor-formula-effective-multiplication-factor/ (cit. on p. 23).

[17] Wikipedia. *Geometric and material buckling*. [Online; accessed 11-June-2025]. URL: https://en.wikipedia.org/wiki/Geometric_and_material_buckling (cit. on p. 24).

[18] Nuclear Power. *Effective Delayed Neutron Fraction - β_{eff}*. Accessed: 2025-06-05. URL: https://www.nuclear-power.com/nuclear-power/fission/delayed-neutrons/effective-delayed-neutron-fraction-%CE%B2eff/ (cit. on p. 25).

[19] A. Haghighat. *Monte Carlo Methods for Particle Transport*. Accessed: 2025-08-26. Boca Raton, FL: CRC Press, 2015. ISBN: 978-1-4665-9253-7 (cit. on p. 26).

[20] D. Mancusi et al. *Overview of TRIPOLI-5, a Monte Carlo code for HPC*. EPJ N 10 (2024) 26. DOI: https://doi.org/10.1051/epjn/2024028 (cit. on pp. 29, 32).

[21] S. Anim-Sampong, E.H. K. Akaho, H.O. Boadu, J.DK. Intsiful, S. Osae. *Fuel depletion analyses for the HEU core of gharr-1; Part II: Fission product inventory*. Tech. rep. [Accessed: 2025-06-18]. Dept. of Nuclear Eng. & Mat. Sci., NNRI, National Centre for Mathematical Sciences, Dept. of Physics, NNRI, Ghana Atomic Energy Commission P.O. Box LG 80, Legon, Accra. Ghana (cit. on p. 42).

[22] Wikipedia. *Radioactive decay*. [Online; accessed 19-June-2025]. URL: https://en.wikipedia.org/wiki/Radioactive_decay (cit. on p. 43).

[23] Wikipedia. *Decay chain*. [Online; accessed 23-June-2025]. URL: https://en.wikipedia.org/wiki/Decay_chain (cit. on p. 44).

[24] Wikipedia. *Bateman equation*. [Online; accessed 19-June-2025]. URL: https://en.wikipedia.org/wiki/Bateman_equation (cit. on p. 45).

[25] S. Lahaye, A. Tsilanizara, P. Bellier, T. Bittar. *Implementation of a CRAM solver in MENDEL Depletion Code System*. Tech. rep. cea-02438382f. [Accessed: 2025-06-20]. International Conference on Mathematics, Computational Methods Applied to Nuclear Science, and Engineering (M&C - 2017), Apr 2017, Jeju, South Korea (cit. on p. 47).

[26] International Atomic Energy Agency. *Cumulative Fission Yields*. Accessed: 2025-07-07. URL: https://www-nds.iaea.org/sgnucdat/c3.htm#92-U-235 (cit. on p. 51).

[27] International Atomic Energy Agency. *Independent Fission Yields*. Accessed: 2025-08-06. URL: https://www-nds.iaea.org/sgnucdat/c2.htm#92-U-235 (cit. on p. 52).

[28] International Atomic Energy Agency. *Cumulative Fission YieldActinide data: Thermal neutron cross sections, resonance integrals, and Westcott factors*. Accessed: 2025-07-07. URL: https://www-nds.iaea.org/sgnucdat/a5.htm (cit. on p. 53).

[29] E. Deville and F. Perdu. *Documentation of the interface for code coupling: Icoco. D3.3.1.2, NURISP, 2012*. Tech. rep. [Accessed: 2025-06-26] (cit. on pp. 56, 57).

[30] *C3PO (Collaborative Code Couling PlatfOrm)*. [Online; accessed 2025-06-30]. URL: https://salome-c3po.readthedocs.io/en/latest/index.html (cit. on p. 58).

[31] *A review of nuclear thermal propulsion carbide fuel corrosion and key issues Final Report*. Tech. rep. Accessed: 2025-08-19. NASA, 1975 (cit. on pp. 64, 65).

[32] Ontosight. *T Test and 0.05 Significance Level*. Accessed: 2025-07-08. URL: `https://ontosight.ai/glossary/term/T-Test---two-tail` (cit. on p. 72).

List of Acronyms

AEC Atomic Energy Commission

API Application Programming Interface

CEA Commissariat à l'énergie atomique et aux énergies alternatives

CFY Cumulative thermal Fission Yields

C3PO Collaborative Code Coupling PlatfOrm

eV Electron volts

GENDF Groupwise Evaluated Nuclear Data File

HPC High Performance Computing

ICoCo Interface Code Coupling

IFY Independent fission yields

IRSN Institut de Radioprotection et de Sûreté Nucléaire

LH2 Liquid hydrogen

LOx Liquid oxygen

MC Monte Carlo

MPI Message Passing Interface

NERVA Nuclear Engine for Rocket Vehicle Application

NTP Nuclear Thermal Propulsion

pcm Per cent mille

RW Random Walk

SALOME Simulation numérique par Architecture Logicielle en Open source et à Méthodologie d'Evolution

SNRE Small Nuclear Reactor Engine

T-4 TRIPOLI-4

T-5 TRIPOLI-5

List of Symbols

General Physics Symbols

Symbol	Definition	Units
F	Force	N
g_0	Standard gravity	m/s^2
I_{sp}	Specific impulse	s
M	Molar mass of gas	g/mol
p	Absolute inlet gas pressure	Pa
p_e	Absolute outlet gas pressure	Pa
R	Universal gas constant	$J/(mol \cdot K)$
T	Combustion chamber temperature	K
v_e	Exhaust velocity	m/s

Nuclear Physics and Reactor Parameters

Symbol	Definition	Units
A	Mass number	AMU
$b_{k \to i}$	Branching ratio	–
β	Delayed neutron fraction	–
β_{eff}	Effective delayed neutron fraction	–
λ	Decay constant	s^{-1}
k_{eff}	Effective multiplication factor	–
k_{inf}	Infinite multiplication factor	–
N	Nuclei density	$\mathrm{nuclei/cm}^3$
N_{A}	Avogadro's number	mol^{-1}
ν	Avg. neutrons per fission	–
ϕ	Neutron flux	$\mathrm{n/(cm}^2 \cdot \mathrm{s)}$
ρ	Reactivity	–
Σ	Macroscopic cross section	cm^{-1}
σ	Microscopic cross section	cm^2
$T_{1/2}$	Half-life	s
v	Neutron velocity	cm/s

Chemical Elements and Particles

Symbol	Definition	Units
Al	Aluminum	–
B	Boron	–
Ba	Barium	–
Cd	Cadmium	–
Co	Cobalt	–
C	Carbon	–
Cs	Cesium	–
Cu	Copper	–
Fe	Iron	–
Gd	Gadolinium	–
H	Hydrogen	–
He	Helium	–
I	Iodine	–
Li	Lithium	–
N	Nitrogen	–
Ni	Nickel	–

Symbol	Definition	Units
Np	Neptunium	–
Pu	Plutonium	–
Rb	Rubidium	–
Sr	Strontium	–
Th	Thorium	–
U	Uranium	–
Xe	Xenon	–
Zr	Zirconium	–
α	Alpha particle	–
γ	Gamma photon	–
n	Neutron	–
p	Proton	–
e^-	Electron	–
$\bar{\nu}_e$	Antineutrino	–

Other Symbols

Symbol	Definition	Units
I	Importance	–
ψ	Random sample	–